Experimental observations of marine iodide oxidation using a novel sparge-interface MC-ICP-MS technique

D.S. Hardisty[1,2,3], T.J. Horner[2,4], S.D. Wankel[4], J. Blusztajn[2,3], and S.G. Nielsen[2,3]

[1]Department of Earth and Environmental Sciences, Michigan State University, East Lansing, MI, USA
[2]NIRVANA laboratories; [3]Department of Geology and Geophysics; [4]Department of Marine Chemistry, Woods Hole Oceanographic Institution, Woods Hole, MA, USA

Abstract

Iodine speciation is used as a redox indicator and water mass tracer. However, the kinetics and mechanisms of oxidation of the reduced iodine species, iodide (I^-), in seawater remain largely unresolved. Here, we provide constraints on I^- oxidation rates from seawater incubation experiments using a sensitive radiotracer–incubation approach with high-precision mass spectrometry. Samples are inoculated with iodine-129 as I^-, incubated under controlled conditions, then oxidized and reduced iodine species are isolated using liquid chromatographic separation. Samples are subsequently aspirated using a novel sparging interface, and the $^{129}I/^{127}I$ ratio of both iodine species are determined via multi-collector inductively-coupled plasma mass spectrometry. This highly-sensitive analytical approach is optimized for estimating the predicted slow rates of iodine redox transformations in small volume seawater samples at marine-relevant total iodine concentrations. Application of this method to coastal samples from Martha's Vineyard Sound, USA, evidences the heretofore-elusive oxidation of I^- under marine-analogue conditions. Our results demonstrate an increase in the $^{129}I/^{127}I$ of aqueous oxidized iodine species in unamended seawater, most likely due to formation of hypoiodous acid and then dissolved organic iodine, at rates of 118–189 nM yr^{-1}. These rates are comparable to those inferred from previous open ocean mass balance approaches but have the benefit of directly linking iodine speciation changes to *in situ* I^- oxidation. Though our treatment experiments do not definitively isolate the oxidation mechanism, they provide preliminary insight into important roles for both abiotic and biotic factors as well as iodine transformations between dissolved, particulate, and gaseous forms. Ultimately, the derived rates and novel experimental technique have potential to improve marine iodine cycling models and provide constraints on the importance of *in situ* processes in setting patterns of iodine speciation.

Keywords: seawater iodine, iodide oxidation, multi-collector inductively-coupled plasma mass spectrometer, paleoredox proxy

1. Introduction

The speciation of dissolved iodine has been applied as a tracer for the redox state of modern (Cutter et al., 2018; Farrenkopf and Luther, 2002; Luther and Campbell, 1991; Rue et al., 1997; Wong and Brewer, 1977; Wong et al., 1985) and ancient regional seawater masses (Hardisty et al., 2017; Hardisty et al., 2014; Hoogakker et al., 2018; Lowery et al., 2018; Lu et al., 2018; Lu et al., 2016; Lu et al., 2010). The major iodine species dissolved in seawater—iodate (IO_3^-), iodide (I^-), and dissolved organic iodine (DOI)—typically sum to 450-500 nM (Chance et al., 2014). Ancient dissolved IO_3^- can be traced through the composition of iodine in carbonate rocks, which have been demonstrated to specifically precipitate with IO_3^- in the carbonate lattice (Feng and Redfern, 2018; Kerisit et al., 2018; Lu et al., 2010; Podder et al., 2017). Work in modern systems has proven the usefulness of IO_3^- and other iodine species as potential

seawater redox tracers, as IO_3^- requires O_2 for accumulation and is quantitatively reduced to I^- in reducing settings such as oxygen deficient zones and anoxic basins (Cutter et al., 2018; Farrenkopf and Luther, 2002; Luther and Campbell, 1991; Rue et al., 1997; Wong and Brewer, 1977; Wong et al., 1985). However, quantitative applications of marine IO_3^- (and iodine speciation generally) as a tracer of marine redox in modern and ancient systems are ultimately hindered by limited constraints on marine I^- oxidation and a complete lack of observations of marine IO_3^- formation in experimental systems. The purpose of this study is to provide a pathway forward to fill this gap.

The distributions of each of the major iodine species in seawater are well described in the modern ocean, with distinct patterns characterizing marine euphotic (Chance et al., 2014), pore water (Anschutz et al., 2000; Kennedy and Elderfield, 1987a; Kennedy and Elderfield, 1987b; Ullman and Aller, 1985), low oxygen environments (Cutter et al., 2018; Farrenkopf and Luther, 2002; Luther and Campbell, 1991; Rue et al., 1997; Wong and Brewer, 1977; Wong et al., 1985), among others. As is predicted from thermodynamic calculations, the oxidized iodine species, IO_3^-, dominates in well-oxygenated settings, and nearly quantitatively represents total dissolved marine iodine in aphotic offshore waters (Luther et al., 1995). However, I^-/IO_3^- are not in thermodynamic equilibrium in euphotic waters and I^- represents up to 50% of total iodine in these settings (Chance et al., 2014). Additionally, DOI and I^- are each elevated in near-shore settings. In some coastal waters, DOI represents up to 80% of total dissolved iodine (Wong and Cheng, 1998; Wong and Cheng, 2001a; Wong and Cheng, 2001b; Cook et al., 2000; Wong and Cheng, 2008). Multiple previous studies have provided theoretical and experimental constraints on the oxidation of marine I^- to intermediate iodine species (Reactions 1-6). For example, it is known that O_2 is not a direct oxidant of I^-, but instead stronger oxidants such as reactive oxygen species and ozone are required (Carpenter et al., 2013; Küpper et al., 2008; Li et al., 2014; Luther et al., 1995; Sherrill et al., 2004; Wong and Zhang, 2008). The oxidation of I^- has been demonstrated to proceed via intermediate iodine species, specifically hypoiodous acid (HOI) and molecular iodine (I_2), which are in equilibrium with one another in seawater (Truesdale and Luther, 1995). These intermediate iodine species are both gaseous when formed from ozone reactions at the air–sea interface (Carpenter et al., 2013) and dissolved HOI is highly reactive with dissolved organic carbon (DOC) to form dissolved organic iodine (DOI) species (Reaction 5; Bichsel and Von Gunten, 1999; Truesdale and Luther, 1995; Luther et al., 1995). Beyond volatilization and reactions with DOC, HOI is also known to disproportionate to IO_3^- and I^- (Reaction 6), though this reaction is considered to be negligible in seawater (Truesdale, 1974; Truesdale and Luther, 1995). The oxidation of I^- (Fox et al., 2009; Li et al., 2014; Li et al., 2012) and subsequent organic-iodine formation (Santschi et al., 2017; Schwehr et al., 2005; Xu et al., 2013) has been studied extensively in freshwater systems (reviewed in Yeager et al., 2017); however, experimental constraints on marine I^- oxidation and DOI formation under normal marine conditions remain limited. Together, the strong oxidants necessary for I^- oxidation and the reactivity of HOI with DOC to form DOI likely act as bottlenecks for direct observations of I^- oxidation to IO_3^- in seawater.

$H^+ + I^- + O_3 \rightarrow HOI + O_2$	Reaction 1
$I^- + H_2O_2 \rightarrow HOI + OH^-$	Reaction 2
$2I^- + 2H^+ + H_2O_2 \rightarrow I_2 + 2H_2O$	Reaction 3
$HOI + I^- + H+ \leftrightarrow I_2 + H_2O$	Reaction 4
$I_2/HOI + R \rightarrow I\text{-}R$ (R=organic moieties)	Reaction 5
$3HOI \rightarrow IO_3^- + 2I^- + 3H^+$	Reaction 6

Isotope labeled tracers represent a powerful means to track and quantify reactions in seawater (Dugdale and Goering, 1967; Jørgensen, 1982; Moffett, 1990; Moffett and Ho, 1996). Iodine has 37 known isotopes (Audi et al., 2003), but only one stable isotope, ^{127}I. While all other radiogenic iodine isotopes have half-lives on the scale of months to less than seconds, ^{129}I has by far the longest half-life ($t_{1/2}$~15.7 Ma). As such, the long half-life of ^{129}I ultimately allows its use as a stable tracer on short timescales (<decades), as has already been demonstrated in open ocean settings (Buesseler et al., 2017;

Hansen et al., 2011; Hou et al., 2007; Hou et al., 2001; Hou et al., 2013).

Here we provide experimental observations of I^- oxidation in seawater and associated rates via ^{129}I tracer-doped seawater incubations. Treatments are performed in light and dark and under filtered and unfiltered conditions in order to constrain photic- and biologic-specific pathways. We also demonstrate a novel sparge-based introduction system of iodine gas into a multicollector-inductively coupled plasma mass spectrometer (MC-ICP-MS) for the precise measurement of $^{129}I/^{127}I$ ratios.

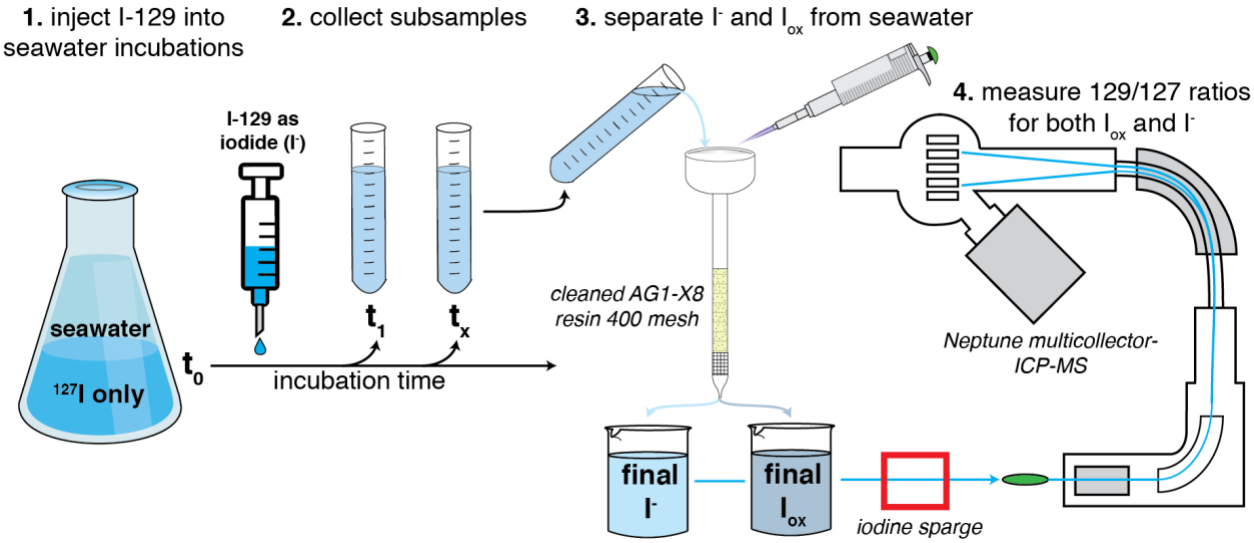

Fig. 1. Generalized schematic outlining the iodide-129 incubation experiments. The experiments integrate the adapted iodine speciation separation technique and the novel sparge MC-ICP-MS techniques. The premise of the incubations is that an increase in $^{129}I/^{127}I$ ratios in DOI or IO_3^- can be linked back to oxidation of the iodide-129 tracer.

2. Mass spectrometry, chromatography, and experimental protocols

2.1 Reagents

The iodide-127 standard used was a 999±4 mg/L solution in 1% tetraethylammonium (TEA) from Inorganic Ventures©. The iodate-127 standard is an ACS-grade potassium iodate powder from Acros©. All IO_3^- and I^- solutions were gravimetrically prepared using 18.2 MΩ cm^{-2}-grade water from a Milli-Q system (MilliporeSigma©) in the Class 100 NIRVANA Lab clean room at WHOI (Woods Hole Oceanographic Institution).

An iodide-129 solution—hereinafter referred to as the 'spike'—was purchased from Eckert and Ziegler Isotope Products©, which had been calibrated via a liquid scintillation counter to have an activity of 0.3681 kBq/g with ±3.3% uncertainty in a 10 mL solution. The solution was in a NaI carrier solution in 0.1 M LiOH; the ^{127}I content of the carrier solution and thus the $^{129}I/^{127}I$ ratio of the spike were not specified by the manufacturer.

Additional solutions include: a Te standard containing 1000 mg/L Te in 0.75 M nitric acid (Assurance©). Acros Organics© 99% extra pure potassium nitrate; Acros© ACS-grade sodium bisulfide; Alfa Aesar© 25% w/w aq soln. Electronic Grade (99.9999%) tetramethylammonium hydroxide (TMAH); Fischer Scientific© certified ACS plus nitric acid; Fischer Scientific© ACS plus hydrochloric acid.

2.2 Incubation experiments

Seawater was collected from Martha's Vineyard Sound at WHOI's Environmental Systems Laboratory (ESL). ESL intakes seawater from polypropylene pipes located approximately 200 m offshore from WHOI's Quissett Campus where water depths reach ~5 m. The pipes are located at approximately 0.5 m from the bottom and contain approximately 2.5 cm mesh to filter out fish and other larger material. Salinity and pH of the intake and output water are consistently near 31 and 7.9, respectively, including at the time of the study. Dissolved organic carbon concentrations were not quantified at the time of the study but have been previously recorded to range up to 115 µM in Martha's Vineyard Sound (Hopkinson et al., 2002). These values are similar to that observed for Chesapeake Bay (Hopkinson et al., 2002), where measurements of I^-, IO_3^-, and DOI suggest up to 50% of the total dissolved iodine is represented by DOI (Wong and Zhang, 2003).

We performed four separate incubation treatments. A large t_0 batch was made for each experimental treatment, but each individual time point was allocated into a separate incubation vial, such that incubations were performed individually for each time point. Each treatment included independently incubated duplicates for each time point (10 mL). A t_0 sub-sample was collected immediately following the addition of the ^{129}I spike and sub-samples were harvested periodically over the course of 67 days. In order to prevent de-oxygenation and subsequent IO_3^- reduction, the seawater was kept aerated through the use of loose caps, which minimized any contamination through airborne particles, but maintained equilibrium between the headspace and ambient atmosphere. The incubations were maintained on a shaker table at 180 rpm through the duration of the experiment.

The treatments from seawater collected from the ESL coastal station included: **A.)** Unamended seawater; **B.)** Seawater passed through passive sand-bed filtration (~0.5 mm) which is intended in comparison to Incubation A to determine the role of particles or other native macro-materials in iodine speciation changes while still maintaining similar microbiology to unamended seawater; **C.)** a "kill treatment" which consisted of seawater passed through a 0.22 µm-filter and subsequently irradiated with UV light at 254 nm to induce thymine dimerization, which does not destroy but inactivates microorganisms. Also, irradiation has been shown to reduce DOC contents

and associated DOI (Wong and Zhang, 2008). **D.)** 18.2 MΩ cm^{-2}-grade H_2O spiked with the same levels of ^{129}I and incubated alongside the other incubations, which was used as a control and to quantify contamination from other external iodine sources.

Incubations were conducted under both ambient laboratory light near an uncovered window and dark (foil covered) conditions, all at room temperature. For each experiment, the ^{129}I spike was gravimetrically added as I^- at levels adding a total of 700-800 nM extra I^- to the seawater, allowing for quantification of initial seawater I^- concentrations. These I^- concentrations are elevated relative to dissolved total iodine in most marine waters (450-500 nM) but are within a range found in rare cases in some deep marine waters and are typical of pore waters (Chance et al., 2014; Cutter et al., 2018; Farrenkopf and Luther, 2002). Outside of OMZ settings, where I^- can quantitatively represent total dissolved iodine, concentrations of I^- are typically <150 nM (Chance et al., 2014). The extra I^- beyond typical seawater in our experiments was added in order to ensure a sufficient I^- concentration for the reactions but was purposefully kept far below levels known to stimulate brine-specific iodine oxidizing bacteria, or 63-1200 µM I^- (Amachi et al., 2005).

Upon harvesting each time point, samples were immediately filtered (0.22 µm syringe-filter) and stored at 4˚C to maintain speciation (Campos et al., 1996; Farrenkopf et al., 1997). The oxidized iodine, or I_{OX} (IO_3^- + dissolved organic iodine), and I^- were separated according to the chromatographic method described below. For the unamended seawater and "kill treatment" the time points were put through the chromatographic separation <7 days after collection. For the passive sand-filtered seawater, all of the time points were chromatographically separated for iodine speciation at the same time 4 days after the collection of the final time point. The isotope ratios of I_{OX} and I^- were measured primarily via the sparge technique described below, but for comparison a few samples were also measured via an existing wet plasma method. The calibration of the iodine-129 spike is outlined in detail in the next sections. Concentrations of ^{127}I were determined on some samples on the Thermo iCAP ICP-MS. Given no means to monitor overall yields from the column chemistry procedure (such as ^{125}I; Hou et al., 2001), the iCAP concentration measurements are used to qualitatively assess changes in concentration during the experimental incubations and as an aid to interpreting the isotope trends.

2.3 Iodine purification

The method for separating and purifying dissolved iodine species is outlined in Figure 2 but is derived from ion-exchange chromatographic approaches widely used in the literature to separate DOI, IO_3^-, and I^- from natural waters (Hou et al., 2007; Hou et al., 2009; Hou et al., 2001; Hou et al., 1999; Hou et al., 2013; Reifenhäuser and Heumann, 1990; Wong and Brewer, 1976). The previous technique utilizes a 2.0 M KNO_3 solution for elution of I^- from the columns. For the sample sizes utilized in this (<10 mL) or other practical incubation studies, the necessary dilutions to analyze iodine concentrations in the described KNO_3 matrix via MC-ICP-MS or ICP-MS are too extreme to render iodine detectable. Here, instead of KNO_3 and $NaNO_3$ used in the previous techniques, we elute the retained I^- by addition of 2M HNO_3, which effectively strips I^- from the anion exchange resin. In order to stabilize iodine in solution, TMAH can be added, which prevents oxidation to HOI/I_2 and subsequent loss via volatilization and represents the matrix frequently used for measurement of iodine via ICP-MS and MC-ICP-MS (Chai and Muramatsu, 2007; Isnard et al., 2016; Lu et al., 2010; Santamaria-Fernandez et al., 2006). Prior to the calibration of the chromatographic procedure, we performed an experiment to determine the amount of TMAH necessary for addition to a 2 M nitric acid eluent in order to prevent iodine volatilization and found that 18% (vol/vol) TMAH was required to keep iodine stable in solution over time scales of days to months (Supplementary Fig. 1).

Under the described conditions, iodine is eluted as I^- following <15 mL of 2M HNO_3–18% TMAH eluent additions (Supplementary Fig. 2). Nearly 100% of the iodine is eluted within the

194 4^{th}-10^{th} mL and ~85% in the 4^{th}-7^{th} mL. The recovery we obtain here is very similar to those
195 reported elsewhere that were in the range of 80-98% (Hou et al., 2007; Hou et al., 2001). As in
196 these previous studies, once the DOI and IO_3^- fractions are separated from the seawater I^-, these
197 fractions are externally reduced to I^- via acidification and addition of sodium bisulfite, and then
198 added to the same column procedure (Fig. 2).

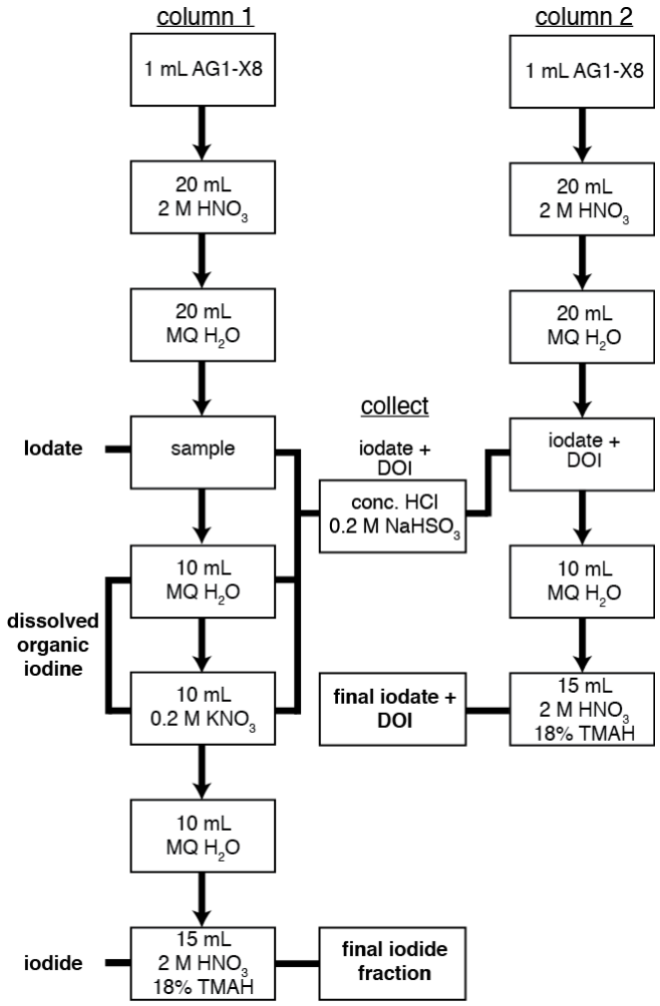

199 **Fig. 2.** Individual steps for chromatographic separation of iodide, dissolved organic iodine, and
200 iodate from seawater. The volume of eluent required has been determined as part of this study,
201 but the separation technique is generally informed and adapted from a previously developed
202 method (Hou et al., 2009; Hou et al., 1999; Reifenhäuser and Heumann, 1990). The final
203 fractions are in bold. Unless otherwise indicated, the added solutions are not collected.

2.4 Iodine Isotopic Analyses

All iodine isotope ratios were measured on a ThermoFinnegan Neptune MC-ICP-MS at the WHOI Plasma Facility. Ion beams corresponding to *m*/*z* 126 (Te, Xe), 127 (I), 128 (Te, Xe), 129 (I, Xe), 130 (Te, Xe), 131 (Xe), and 132 (Xe, Ba) were simultaneously monitored in low resolution mode in Faraday cups L3-L1 and H1-H3 with *m*/*z* 129 in the center position. All detectors were assigned 10^{11} Ω resistors, except for those measuring *m*/*z* 127 and 129, which were episodically switched between the one 10^{10} Ω resistors on account of their much larger signal intensities. We used a regular sample cone and an x-type skimmer cone. Radio frequency power was found to be optimal when maintained at 1,350 W (Santamaria-Fernandez et al., 2006), with auxiliary and cooling gas flow rates ≈ 1 and 16 L/min, respectively. These parameters, in addition to focusing lenses, were regularly tuned to improve peak overlap, shape, and overall ion beam intensity.

Tellurium is used to characterize instrumental mass fractionation and Xe is monitored (on *m*/*z* 131) to correct for spectral overlap with iodine and Te. The former causes measured $^{129}I/^{127}I$ ratios to deviate from 'true' values by several percent; the latter is present as a trace impurity in the argon carrier gas used on ICP-MS instruments (Horner et al., 2015). Careful correction is required to avoid misattribution of measured ion beam intensities—and specifically those of *m*/*z* 129—to iodine redox transformations rather than analytical artifacts. In the course of conducting these corrections, both the Te in our standard and Xe present in the argon carrier gas were assumed to have mean solar isotope abundances (i.e., ^{126}Te, ^{128}Te, and ^{130}Te representing 0.1884, 0.3174, and 0.3408 of total Te, respectively; ^{126}Xe, ^{128}Xe , ^{129}Xe, ^{130}Xe, ^{131}Xe, and ^{132}Xe representing 0.000890, 0.019102, 0.264006, 0.040710, 0.212324, and 0.269086 of total Xe, respectively (de Laeter et al., 2003)).

We evaluated existing solution-based measurement of $^{129}I/^{127}I$ against a new gas-phase 'sparge' method using standard solutions dissolved in representative matrices. Gravimetric mixtures of ^{127}I standard solution with a known concentration and variable amounts of ^{129}I spike solution were used to calibrate the $^{129}I/^{127}I$ ratio of the spike and the corresponding concentrations of both isotopes in the spike. The use of gravimetric standards also enabled comparison of ion transmission efficiencies (of ^{127}I) under both operating conditions.

2.4.1 Solution-based sample introduction

Unless otherwise specified, all aspects of the MC-ICP-MS tune parameters, Xe correction, Te mass bias corrections, and iodine isotope ratio calculations are maintained as described in the previous and following section. Following a variation of the Santamaria-Fernandez et al., (2006) and Isbard et al. (2016) $^{129}I/^{127}I$ ratio determination methods, we determined the iodine isotope ratio for the ^{129}I spike solution using MC-ICP-MS. Solutions were introduced to the plasma via a 300 µL/min quartz nebulizer. All solutions contained ≤ 4.5% TMAH (v/v). Samples were analyzed for 180 s in ≈ 8 s integrations. We quantified the instrumental mass bias on $^{129}I/^{127}I$ by adding dissolved Te to our spike–standard mixtures to achieve a final [Te] of 100 ng/mL (see Sec. 2.4.3, below, for details regarding data reduction). These solutions were used to characterize the $^{129}I/^{127}I$ ratio of the ^{129}I spike solution at variable ^{129}I intensities, determine the concentration of ^{129}I and ^{127}I via isotope dilution, and characterize blank contributions. Rinse solutions consisted of variable combinations of the matching matrix of the corresponding samples and 1% HBr (Santamaria-Fernandez et al., 2006). Rinses were monitored for all previous mentioned ion beams and new standards or unknowns were not measured until these masses returned to pre-measurement levels, which, at iodine concentrations in the µg/L range, often took >10 minutes. At TMAH concentrations >1.25%, the torch required daily (or more) cleaning due to buildup of a white film on the torch injector, which lowered signal intensities.

2.4.2 Gas-based sample introduction (sparge)

Here, we describe a novel sparge approach that exploits the propensity of iodine to volatilize in the presence of oxidizing agents (e.g., Berry et al., 1987; Isnard et al., 2016; Remenec et al., 2017) as a means of introducing iodine into the mass spectrometer. Doing so has the potential to improve iodine transmission efficiency since iodine is liberated from the TMAH buffer before ionization. This approach is derived from the sample introduction method routinely used at the WHOI Plasma facility for osmium isotope measurements via MC-ICP-MS (Sen and Peucker-Ehrenbrink, 2014). Similar to the wet plasma solution-based technique described in the previous section, we adopt the use of Te as a means of correcting instrumental mass fractionation and we also track Xe isotopes for ^{129}Xe interference corrections. Samples were typically analyzed for 240 s at ≈ 1 s integrations. A conceptual image of the sparge-introduction system is shown in Fig. 3 and detailed below. In each case, the sparged iodine is in the form of I^- (see previous discussion of chromatographic technique).

A Te solution, dissolved in 18.2 MΩ cm^{-2}-grade H_2O, was aspirated at 100 μL min^{-1} with an ESI micro-concentric PFA nebulizer using ≈ 1 L min^{-1} of Ar gas, and desolvated through an ESI Apex Q desolvation system operated in 'hot' mode. The resultant Te aerosol (and Ar propellant) were subsequently bubbled through a sparge vial containing the sample, and the headspace (containing Ar, Te aerosol, and I gas) evacuated into the mass spectrometer. The concentration of Te in the standard solution was modified to maintain Te ion beam intensities < 0.5 pA. The iodine-containing solution is held in a PFA sparge vial (Savillex). Analogous to the Os isotope method (Sen and Peucker-Ehrenbrink, 2014), the sparge vial consists of a PFA container, PTFE tape on the threads, and a PFA cap containing two separate ⅛ inch holes to insert ⅛ inch PTFE tubing for gas input and output from the sparge vial. For the introduction tubing, the tubing should go through the sparge cap, with the end submerged into the sparge solution. The end of the PTFE tubing for bubbling the sparge solution was heated, crimped, and ~10 holes were made in the tubing using a pin at locations which are submerged in the solution. For output from the sparge vial, unmodified PTFE tubing is placed into the output hole of the sparge cap at a length that assures it is adequately above the sparge solution, drawing only from the vial headspace. The ⅛ inch PTFE tubing output from the sparge vial is connected to a ¼ inch silicone tube with a ¼-to-⅛ inch PTFE connector. The silicon tubing is connected to the MC-ICP-MS torch with a glass fitting. Sparge vials, caps, and tubing were cleaned in 50% nitric acid bath and thoroughly rinsed with 18.2 MΩ-grade H_2O before use for each individual sample. The silicon tubing was discarded and replaced between samples to eliminate possible carryover. The ⅛-to-¼ inch PTFE connector, glass fitting, and torch were the only aspects of the introduction system exposed to iodine from samples and standards without being replaced or cleaned between samples.

For analysis, the solution was placed in the sparge vial, and, prior to connecting the glass connector to the torch, Ar and Te gas were run through the sparge introduction system for ~1 minute to evacuate the headspace. Before connecting the glass connector and the torch, the Ar gas flow rate was decreased to <0.15 L min^{-1}. Following connection, the Ar gas flow rate was progressively increased to its optimum flow rate, established during prior tuning, usually 1.1–1.3 L min^{-1}. Once the Ar gas flow rate was at the appropriate value and Te signals were stable, we began monitoring ion beam intensities on the *m*/*z* described in the previous section. These initial analyses recorded prior to the introduction of nitric acid represent the background intensities for correction of memory from previous samples (described in next section). Following background integration for ~20 seconds, the T-valve was turned to allow for the introduction of nitric acid, which was slowly injected into the sparge vial through a syringe. Matrix-matched solutions without iodine additions were analyzed routinely to monitor blanks and memory contributions. We typically added 1-3 mL of nitric acid to 10 mL of sample solution containing 4.5% TMAH. All figures showing iodine volatilization specify the sample volume, % TMAH of the solution, nitric volume added, and (when known) the iodine concentration of the solution.

Observed iodine intensities would frequently exceeded the 50 V 'limit' of the 10^{11} Ω resistors when using the sparge technique. In subsequent cases, where experience indicated this was a possibility, a 10^{10} Ω resistor was placed on either *m/z* 127 or 129, and a new detector gain calibration was performed. If necessary, we further reduced iodine signal intensities by diluting samples to lower iodine concentrations and by adding less nitric acid during sparging.

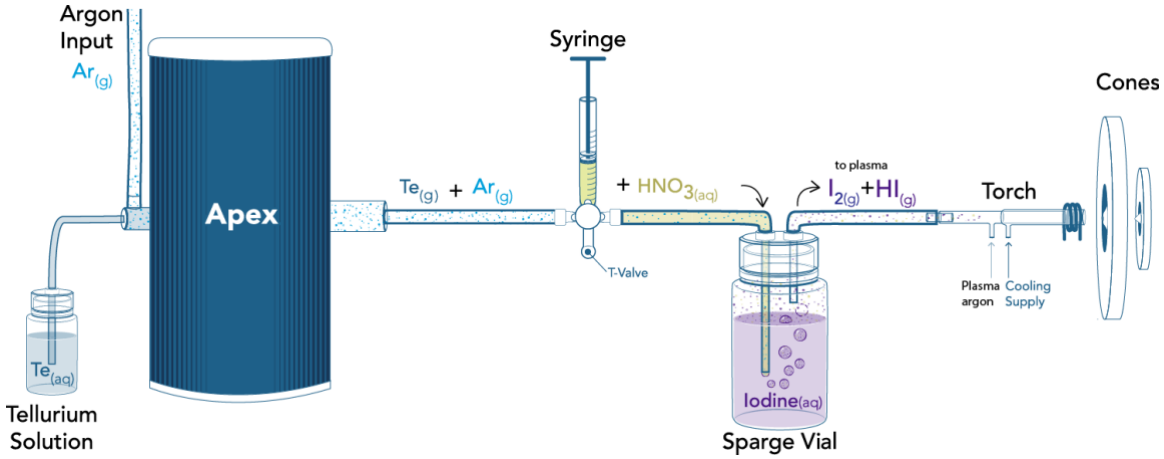

Fig. 3. Iodine sparge illustration. Details are outlined in the main text. The image is courtesy of Natalie Renier, Woods Hole Oceanographic Institution. The Apex is a desolvation system where the solute (in this case water) is removed from the dissolved component (in this case Te) leaving an essentially dry aerosol to be introduced to the mass spectrometer. The point of introduction of Te prior to the sparge vial was explicitly chosen to simplify the changeover process between samples, so a single Ar source escorts both Te and I to the MC-ICP-MS.

2.4.3 Data reduction

'True' isotope ratios, R_t, were assumed to relate to measured ratios, R_m, through the exponential law (e.g., Belshaw et al., 1998):

$$R_t = R_m \, (m_1 / m_2)^f \qquad \textit{(Equation 1)}$$

Where m_1 and m_2 represent the exact masses of the isotopes of interest (e.g., $^{130}Te/^{126}Te$, $^{129}I/^{127}I$) and f is the atomic mass unit-normalized instrumental mass bias correction factor. For both the solution- and gas-phase measurements, f was calculated from $^{130}Te/^{126}Te$ and would henceforth be used to correct instrumental mass bias for other isotope ratios of interest.

The value of f calculated from measured $^{130}Te/^{126}Te$ is both important to—and itself depends upon—the correction of Xe spectral interferences. Xenon is present as a trace impurity in the Ar carrier gas (Horner et al., 2015; Ohno et al., 2013) and low intensity Xe ion beams were observed during all analytical sessions (≤ 10 mV on *m/z* 131). As such, the initial value of f, determined from Xe-uncorrected $^{130}Te/^{126}Te$, was used to calculate instrumental mass bias-corrected $^{131}Xe/^{130}Xe$ and $^{131}Xe/^{126}Xe$ (and $^{131}Xe/^{129}Xe$) ratios. These mass bias-corrected ratios were then used to correct $^{130}Te/^{126}Te$ for Xe, enabling recalculation of f using Xe-corrected $^{130}Te/^{126}Te$. This

corrective process was iterated until convergence. The resultant value of *f* was then used to correct measured $^{129}I/^{127}I$ for both instrumental mass fractionation and spectral overlap from Xe (on *m*/*z* 129).

For the sparge method, the median value of *f* obtained from $^{130}Te/^{126}Te$ prior to nitric acid addition was used to correct all subsequent isotope ratios obtained for that sample. (Note that, prior to spike addition, values of *f* determined using Xe- and mass bias-corrected $^{130}Te/^{128}Te$ or $^{128}Te/^{126}Te$ are essentially identical to those determined from $^{130}Te/^{126}Te$.) The decision to use the background region for mass bias corrections was made after observing anomalous values of *f* after nitric acid addition. Specifically, unreasonably large changes in *f*—oftentimes implying a reversal in the sense of instrumental mass fractionation—would occur immediately following nitric acid addition. These unreasonable values of *f* would then return to their background region values after several minutes of analysis. Since iodine ion beam intensities generally peak immediately after nitric acid addition, we hypothesized that the cause of the variability in *f* results from formation of $^{129}I^{1}H^{+}$. Iodine hydrides would cause spectral overlap with Te and be most pronounced when iodine ion beam intensities are highest. Support for this hypothesis comes from the similarly unreasonable variations in *f* that were observed when measuring ^{127}I-rich solutions and incorporating ^{128}Te into the instrumental mass bias calculation. Regardless, we found only minor differences between quantification of $^{129}I/^{127}I$ when using *f* determined from the background region and *f* using an integration-by-integration approach.

A final $^{129}I/^{127}I$ ratio was calculated for each analysis following corrections for background iodine contributions (on *m*/*z* 129 and 127), spectral overlap of ^{129}Xe on ^{129}I, and instrumental mass bias. Final ratios were weighted on an integration-by-integration basis founded on iodine beam intensities. The use of weightings was justified given the significant-but-systematic decay in iodine ion beam intensities over the course of an analysis. This decay follows an exponential trajectory, similar to that reported for osmium isotope analyses conducted via sparging (Sen and Peucker-Ehrenbrink, 2014). As such, weightings were ascribed based on the square-root of the Xe- and memory-corrected ^{129}I ion beam intensity; a four-fold reduction in signal intensity would yield a two-fold reduction in the accompanying weighting. Iodine ion beam intensities that were below the limit of detection—defined here as being less than three times the standard deviation above the blank iodine ion beam intensity measured during background characterization—were ascribed a weighting of zero. All integrations occurring before the peak of iodine ion beam intensity were similarly ascribed a zero weighting, as were all integrations falling below 60 % of said peak intensity.

Henceforth, we will refer to the final, weighted $^{129}I/^{127}I$ of I_{OX} and I^- as R_{OX} and R_{iodide}, respectively.

Sources of uncertainty were investigated independently, but ultimately integrated. These sources include: 1.) variability in $^{129}I/^{127}I$ ratios over the course of the measurement interval; 2.) memory contributions of ^{129}I and ^{127}I from previous samples run on the MC-ICP-MS; 3.) blank contributions of ^{127}I from chromatography and matrix solutions; and 4.) $^{129}I/^{127}I$ ratios of replicate samples independently incubated and processed as part of the experiments.

No correction is made for radioactive decay of ^{129}I over the course of the experiments, as this constitutes an insignificant portion of the observed variability ($t_{1/2}$~15.7 Ma).

3. Results

3.1 Validation of MC-ICP-MS gas-based sample introduction

Our goals for the sparge technique were to: improve transmission into the MC-ICP-MS by introducing iodine as iodine gas (I_2), compare intensities between the sparge and solution

technique, and evaluate the stability of $^{129}I/^{127}I$ isotope ratios over prolonged intervals. Results in Figs 4 and 5 illustrate the change in iodine ion beam intensities following the addition of concentrated nitric acid into the sparge system. In all cases an immediate increase in iodine ion beam intensities, which peaks and decays over the course of the analyses, is observed with the addition of nitric acid. The rate and timing for each the increase, peak, and decay of the signal is a function of the concentration of nitric acid added relative to the matrix and iodine contents. This is demonstrated in Fig. 4a, where variable amounts of nitric acid exhibit different intensity profiles. Increased nitric acid addition allows for a higher signal intensity to be observed for a shorter duration; likewise, smaller acid additions yielded lower signal intensities over longer durations. In all cases the signal shows an exponential decay. For standards with the same ^{127}I concentration, the sparge method increases the transmission efficiency of iodine by ~10× relative to wet-plasma. Fig. 4b displays a comparison of ^{127}I intensities for a 100 µg/L and 20 µg/L solution between the sparge- and solution-based method.

Fig. 5 also displays the corrected isotope ratios in a standard and seawater incubation sample over the course of 4-minute analyses. Results indicate isotope ratio variability of <0.05% over the course of the bulk of signal integration time period. Integrating the 60% portion of the iodine intensity following the signal peak ultimately captures the highest intensities, thus minimizing any influence from background intensities not easily accounted for with the described Xe correction. Regardless, background ^{129}I and ^{127}I intensities can be corrected for by quantifying the pre-nitric values, which can be subtracted from the intensities following addition of nitric acid, and ^{129}Xe contributions are corrected through monitoring of ^{131}Xe and Te isotope signals.

Typical analytical uncertainties, which consider both the standard deviation of $^{129}I/^{127}I$ ratios measured and memory contributions during the integrated interval, are <0.15% of the $^{129}I/^{127}I$ ratios measured. In most cases, the memory error represents the largest contribution to the overall analytical uncertainty.

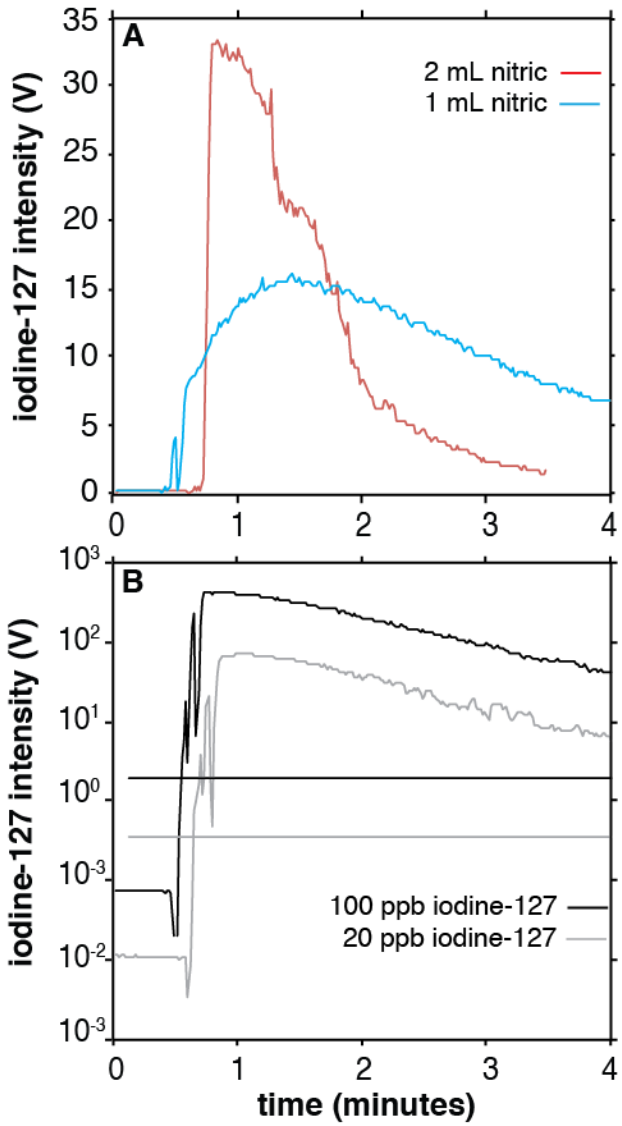

Fig. 4. (A) Plot of the intensity of ^{127}I for two separate runs over the course of a typical analysis interval, with variable volumes of concentrated nitric acid added to volatilize the iodine during sparging. The increase in intensity corresponds to the time of nitric acid addition, as described in the main text. In both cases, an independent 10 mL aliquot of the same solution (9.76 ppb ^{127}I in 1.8% TMAH, 0.2 M nitric acid) was analyzed. **(B)** Comparison of the ^{127}I intensity for the dry plasma, sparge technique (dynamic lines) and wet plasma, solution technique (flat lines) for solutions with ~100 ppb (black) and ~20 ppb (grey). Note difference in scale relative to part A. The increase in ^{127}I for the sparge represents the point of nitric acid addition. For the sparge, 2 mL of nitric acid were added to 10 mL of 1.8% TMAH, 0.2 M nitric acid solution. In each case, the sparge maximum signals are ~200× that from the solution method.

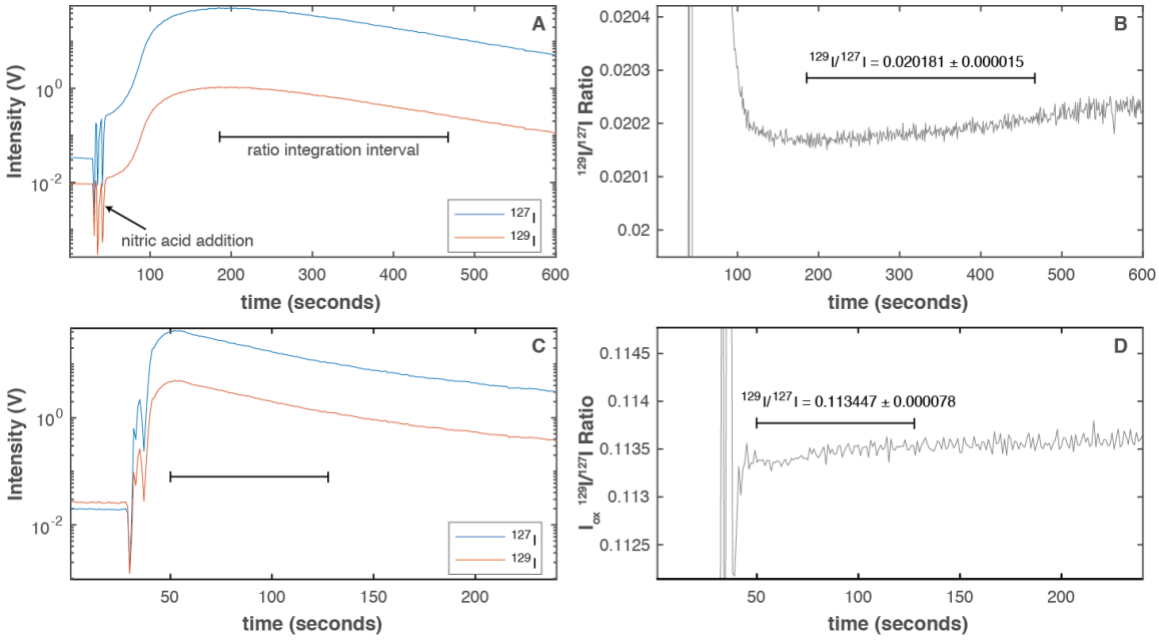

Fig. 5. Isotope ratios from ThermoFinnegan Neptune MC-ICP-MS using the described sparge technique. **(A)** The uncorrected 129 and 127 beam intensities for a gravimetrically blended standard used for determining the ^{129}I and ^{127}I composition of the spike. **(B)** The corrected $^{129}I/^{127}I$ ratio of this same standard. **(C)** The uncorrected 129 and 127 beam intensities for the I_{OX} fraction of a seawater incubation sample. **(D)** The corrected $^{129}I/^{127}I$ ratio for the I_{OX} fraction of a seawater incubation sample. The time of nitric acid addition is represented by the sharp rise in intensities, as shown with the arrow in part A. The pre-nitric intensities represent memory for the ^{127}I and memory but mostly ^{129}Xe interference for ^{129}I. Memory and interference corrections are included in the calculation of the isotope ratios in parts B and D. The horizontal barred line in each figure shows the portion of the signal integrated for $^{129}I/^{127}I$, which is selected based on a standard criterion for all samples, as described in the main text. Approximately 1 mL of acid was added to a 1.8% TMAH, 0.2 M nitric acid standard solution and ~2 mL acid was added to the incubation sample diluted to 4.5% TMAH, 0.5 M nitric.

3.2 Spike calibration

We performed experiments to determine the $^{129}I/^{127}I$ ratio, the relative concentrations of ^{129}I and ^{127}I, and the speciation of the spike. For these experiments, we characterized the $^{129}I/^{127}I$ ratio and ^{129}I and ^{127}I concentrations of an unknown iodine-129 spike using both the new sparge and previously established wet-plasma techniques (Santamaria-Fernadez et al., 2006). Our measurements for the wet-plasma technique include analyses on 3 different days over the course of 2 months and in variable dilutions of the TMAH-nitric matrix and variable ^{129}I concentrations.

The value is 6.28±0.01 (or 0.15% variability; 1σ), which is the value we use to characterize the spike $^{129}I/^{127}I$ isotope ratio.

A mixing line of gravimetric blends of the spike and a certified ^{127}I ICP-MS standard solution (999±4 μg/g) was generated in order to characterize the ^{129}I and ^{127}I concentrations of the spike (Fig. 6). The mixing line was generated to span a range in $^{129}I/^{127}I$ ratios (0.001-0.1) shown in Santamaria-Fernandez et al. (2006) to be optimal for minimizing error propagation. For this mixing line, corrected $^{129}I/^{127}I$ ratios are plotted against the ICP-MS standard ^{127}I concentration relative to the total ^{127}I concentration (spike plus ICP-MS standard). The ^{127}I and ^{129}I contents of the spike represent the unknowns. The ^{129}I concentrations of the gravimetric blends ranged from 0.12-26 μg/L. Using the measured isotope ratios and the concentration of ^{127}I in the ICP-MS standard, we iteratively solved for the ^{127}I concentration of the ^{129}I spike with the constraint of maximizing the coefficient of determination and setting the y-intercept at the determined spike $^{129}I/^{127}I$ ratio (±1σ). The ^{129}I concentration was determined from the calculated spike ^{127}I concentration (±1σ), the gravimetrically determined ^{127}I from the ICP-MS standard, and the measured $^{129}I/^{127}I$ ratio of the gravimetric mixtures. Iodine-127 and ^{129}I concentrations of the spike were found to be 9.39±0.02 mg/L and 53.23±0.83 mg/L (1σ), respectively. The coefficient of determination was 0.99996. This value for ^{129}I concentration overlaps with the concentration of 56.4±1.9 mg/L calculated from the activity of ^{129}I determined by a liquid scintillation counter at Ziegler Isotope Products©.

Lastly, tests were performed to determine the iodine speciation of the spike. We consistently found ^{129}I in the I_{OX} fraction of 18.2 MΩ cm^{-2}-grade H_2O samples inoculated with the ^{129}I spike ($^{129}I/^{127}I$ of 0.23±0.11 1σ for incubation samples). Consistent with this, seawater with additions of the spike contained trace ^{129}I in the I_{OX}-only fraction at t = 0 (Fig. 7), suggesting that the spike contained a small amount of oxidized I. If we assume the I_{OX} pool in the spike has the same $^{129}I/^{127}I$ ratio as the total spike and is mixing with the monitored blank associated ^{127}I, this implies that there is 0.5-0.9 × 10^{-3} mg/L of ^{129}I in the I_{OX} pool of the raw spike, which is about 5 orders of magnitude less than iodide ^{129}I. This I_{OX} could be from IO_3^- or other oxidized forms which are stable in the 0.1 M LiOH spike matrix with NaI carrier. In experiments where sodium bisulfite and HCl were added to spiked solutions, which reduces iodine, this I_{ox} fraction had $^{129}I/^{127}I$ overlapping with that of blanks. The I^- elution fractions from these same experiments also confirmed the overwhelming abundance of I^- in the ^{129}I spike solution.

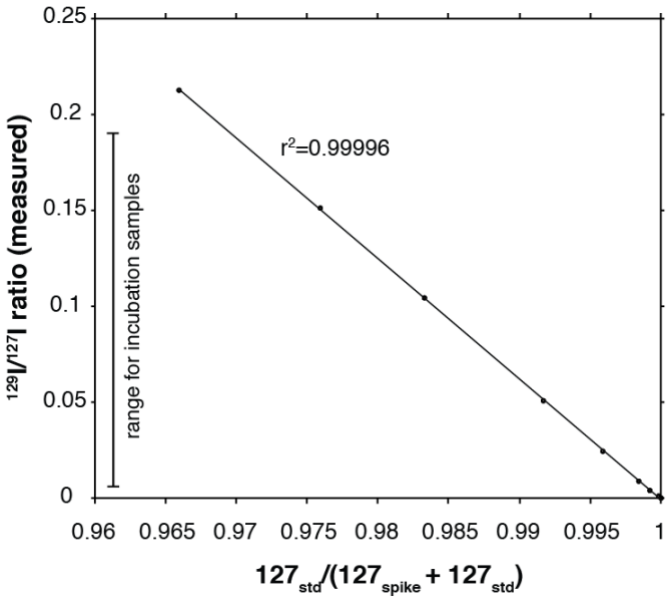

458 **Fig. 6.** The mixing line for gravimetric blends of the ^{129}I spike and the ^{127}I standard as determined
459 via the sparge method, which was used to determine the individual concentrations of each iodine
460 isotope in the spike. Plot shows the measured $^{129}I/^{127}I$ iodine ratio versus the calculated ratio of
461 ^{127}I concentration of the standard and total ^{127}I of the sample. Symbols exceed the size of 3σ on
462 each the y- and x-axis. The ^{127}I of the spike was unknown and solved for iteratively based on
463 constraints maximizing the coefficient of determination and forcing the y-intercept to the
464 determined $^{129}I/^{127}I$ ratio of the spike. The coefficient of determination is 0.99996. Vertical bar
465 shows the range of $^{129}I/^{127}I$ ratios most relevant to the seawater I_{OX} samples from the incubations.

466 ### *3.3 Incubation experiments*

467 All $^{129}I/^{127}I$ and concentration data from this study are available in Supplementary Table
468 1. Measurement of iodine speciation in pre-spiked seawater from the different treatments
469 indicates 90±7 nM I^- and 312±3 nM I_{OX} in treatment A, 196±0.5 I^- and 49±1.5 nM I_{OX} in
470 treatment C, and 4±3 I^- and 16±5 nM I_{OX} in 18.2 2 MΩ cm^{-2}-grade H_2O blanks (Treatment D).
471 The difference in t_0 values between incubations A versus Incubation C most likely reflects direct
472 IO_3^- reduction to I^-, DOI, or gaseous intermediates during the UV-irradiation of the 0.22 µm
473 filtered seawater. A previous study has demonstrated IO_3^- reduction when exposed to light at 254
474 nm wavelength, which was that used here (Brandão et al., 1994; reviewed in Chance et al., 2014).
475 The total iodine concentration near 402 nM for the untreated seawater is similar to the 330-530
476 nM range measured in Chesapeake Bay waters of similar salinity (Wong and Zhang, 2003).
477 A comparison of I^- concentrations determined via isotope dilution from the t_0 samples from
478 each seawater incubation and the I^- concentrations following chromatographic separation were
479 quantified via the Thermo iCAP ICP-MS to determine I^- recoveries for these samples following
480 the chromatographic procedure. Such a comparison indicates that 89-100% of the I^- was
481 recovered. In their original method, Hou et al., (2007) reported recoveries for I^-, I_{OX}, and total
482 dissolved iodine of 80-85%, 90-95%, and 94-98%, respectively. Hou et al., (2001) report
483 recoveries for I_{OX} and I^- of 95.8±4.9 and 94.4±4.2 %, respectively.
484 Values for R_{OX} are shown in Fig. 7. The presence of ^{129}I in the I_{OX} pool of t_0 samples can be
485 explained via observations of trace IO_3^- already present in the spike, as discussed in the previous
486 section. The t_0 samples for R_{OX} have values of 0.0105±0.001, 0.0161±0.001, and 0.0622±0.003
487 (unless specified, all uncertainties ± 3σ) for the unamended (Treatment A), 0.5 mm filtered

(Treatment B), and 0.22 μm filtered/UV irradiated (Treatment C) experiments, respectively. Treatment D had $^{129}I/^{127}I$ for I_{OX} of 0.255±0.001 and 0.207±0.031 for t_1 and t_2, respectively, but was not measured for t_0. Analytical uncertainties are much smaller than the observed $^{129}I/^{127}I$ variations between duplicate samples independently separated for I_{OX} and I^-. The uncertainty estimates represent the 3σ of the $^{129}I/^{127}I$ ratios for the t_0 samples of each individual incubation. The differences in t_0 values among the three experiments are best explained due to differing starting concentrations of seawater I_{OX} (as ^{127}I) for the three treated seawater treatments prior to spike addition.

The unamended and 0.5 mm-filtered seawater experiments reveal a similar increase in R_{OX} for the 67 days of the experiment. For the 0.22 μm-filtered incubations, R_{OX} is observed to increase beyond the range observed for t_0 but to no longer change following the seventh-day time point. No changes in R_{OX} were observed in Incubation D. No consistent difference is observed between light and dark experiments. A decrease in I^- concentrations is observed with time in each experiment measured for concentrations (Fig. 8). The 0.5 mm filtered experiment samples (Treatment B) were not quantified for concentrations because of general similarities between trends in Incubation A. The most useful application of Treatment B is ultimately an additional example of $^{129}I/^{127}I$ increases in R_{OX} (comparable to Treatment A) which are indicative of I^- oxidation. No substantial changes are observed beyond measurement error ranges in I_{OX} as measured via ^{127}I on the ICP-MS (Supplementary Table 1).

The I^- concentrations show a marked decrease over time (Fig. 8a), and a simultaneous decrease in R_{iodide} over the course of the experiments is also observed (Fig. 8b).

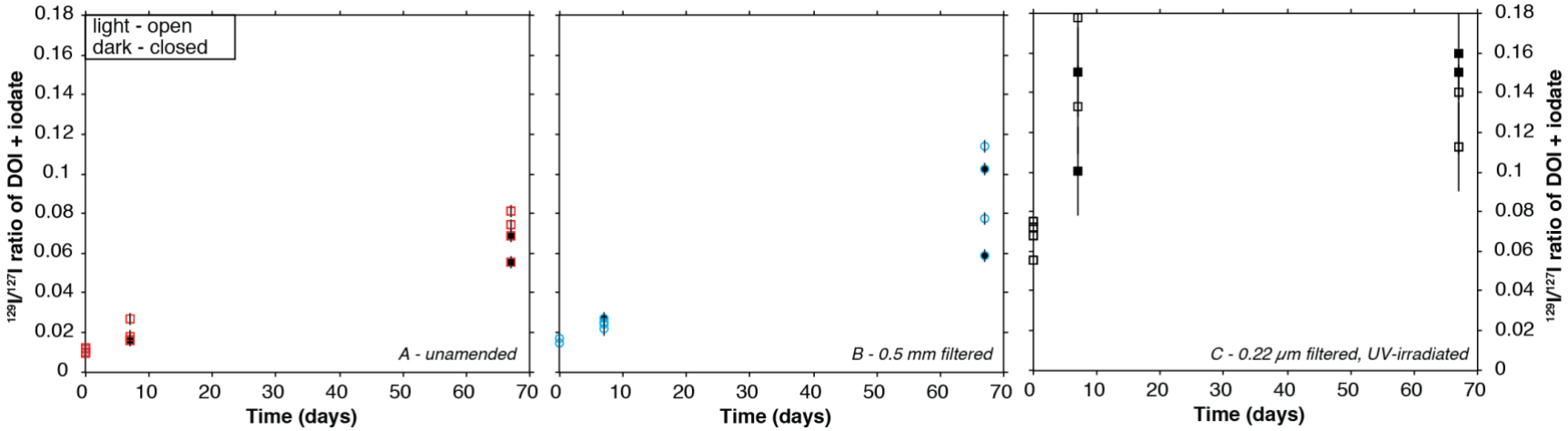

509 **Fig. 7 A.)** The $^{129}I/^{127}I$ ratios for I_{OX} for the **(A)** unamended seawater incubations, (**B)** 0.5 mm filtered seawater incubations, and **(C)** 0.22 µm
510 filtered, UV-irradiated seawater incubations. The error bars given to each sample represent 3σ of the analytical error for each sample. All three
511 incubations were done in duplicate for both light (red) and dark (black) conditions for 67 days. The different t_0 values represent variable initial IO_3^-
512 and DOI as ^{127}I in the treated seawater treatments prior to spike addition.

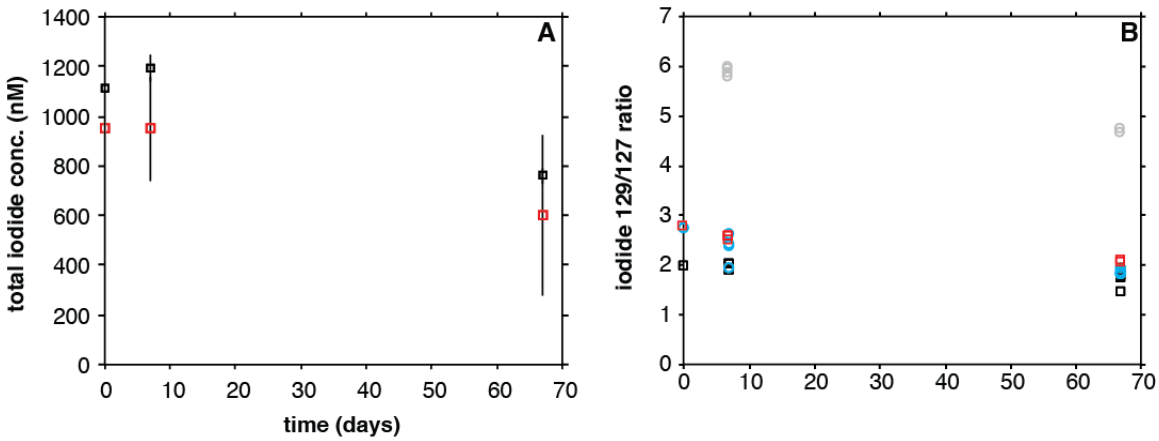

513 **Fig. 8. A.)** Concentrations of I^- from the seawater incubations. The concentration of ^{127}I was
514 measured using an iCAP ICP-MS on the diluted 2M nitric-18% TMAH eluent and then combined
515 with the isotope ratio of the same solutions to determine total I^- ($^{129}I + ^{127}I$). **B.)** Isotope ratios of I^-
516 for each of the experiments. Black squares are from the 0.22 µm-filtered seawater (Treamtent C),
517 red squares from the unamended seawater (Treatment A), blue circles from the sand-filtered
518 seawater (Treatment B), and grey circles are from spiked 18.2 MΩ cm^{-2}-grade H_2O (Treatment
519 D). The light and dark incubated experiments are not differentiated.

520 ## *4. Discussion*

521 ### *4.1 Evaluation of the experimental and analytical approach*

522 In combination with isotope dilution, we anticipate that the novel sparge technique is
523 applicable toward determining iodine concentrations in a variety of other materials beyond
524 seawater using MC-ICP-MS and even ICP-MS. Below we evaluate the sources of uncertainty of
525 the iodine sparge technique and compare it to existing wet plasma solution-based techniques.

526 The combined results from Figures 4 and 5 demonstrate that, through variable nitric acid
527 addition, the iodine intensities can be manipulated and maximized during sparging in order to
528 quantify trace iodine contents. For example, as shown in 4a, higher iodine ion beam intensities
529 can be achieved in samples with anticipated small iodine concentrations—such as those expected
530 for $^{129}I_{OX}$ in our tracer experiments—if the concentration of nitric acid is increased. In contrast,
531 lower nitric acid concentrations can be added for sample measurements where sufficient iodine
532 content requires keeping iodine mass intensities within the detection limits of the selected
533 amplifiers. In addition, for standards with the same ^{127}I concentration, the sparge method
534 increases the transmission efficiency of iodine by ~10× relative to wet-plasma. This is similar to
535 an analogous perchloric acid-based technique for introducing iodine into ICP-MS as a gas (Kerl
536 et al., 1996). The added advantage of the outlined sparge technique is that the majority of iodine
537 from a given sample volume can be evacuated from a liquid and input into the MC-ICP-MS over
538 a shorter time frame, resulting in even higher relative signals (200× relative increase for the
539 example in Figure 4b).

540 The iodine signal decays exponentially, similar to that observed for Os isotopes (Sen and
541 Peucker-Ehrenbrink, 2014), which is what is expected from a first-order reaction whereby the rate
542 of volatilization is proportional to the concentration of iodine in solution. The analytical errors, of
543 <0.15% of the $^{129}I/^{127}I$ ratios measured are similar to that reported previously for the wet plasma
544 technique of <0.1% internal variability (Santamaria-Fernandez et al., 2006). It is important to
545 note that for the incubation experiments, the largest source of error is derived from analyses of
546 duplicate aliquots of single samples put separately through the column chromatography, which is

that used for the purposes of this study. In combination with isotope dilution, we posit that the sparge method has potential to quantify ^{129}I and ^{127}I concentrations from a range of materials beyond that shown here. Analogous nitric-TMAH matrices are used for measurement of iodine contents in organic-rich shales (Zhou et al., 2017), carbonates (Lu et al., 2010), foods (Santamaria-Fernandez et al., 2006), among others. We also expect that alternative matrices are applicable or perhaps even more efficient to what we used here. For example, iodine characterization via sparge and isotope dilution could be ideal for the I/Ca measurement in carbonates with low iodine contents, such as Archean carbonates (Hardisty et al., 2014) or for small sample sizes often required of foraminifera iodine measurements (e.g., Glock et al., 2014; Hoogakker et al., 2018).

We are remaining purposefully cautious in our consideration of DOI and IO_3^- as one pool. Both DOI and IO_3^- represent oxidation products of I^-, with DOI production requiring oxidation of I^- to HOI prior to its formation (Reaction 5; Luther et al., 1995; Truesdale and Luther, 1995). This means that our experiments do provide rates of I^- oxidation, but that we are not currently confident in attributing I^- oxidation to the formation of DOI or IO_3^- individually. Our elution of I_{OX} was consistent with the protocols for the elution of IO_3^- in some previous studies (Hou et al., 1999, 2009; Reifenhäuser and Heumann, 1990); however, neither ours nor previous seawater applications of the same technique have independently validated the lack of DOI input to this elution fraction. Future work should consider providing some secondary characterization—beyond the chromatographic method itself—of the DOI elution component in seawater and for the lack of DOI cross-contamination into the I^- or IO_3^- pools, thus allowing for greater confidence for tracer experiments such as our own to identify the individual formation of these dissolved iodine species.

4.2 Iodide oxidation

Combined with the work of previous studies, our method validation demonstrates the potential to add ^{129}I to seawater incubations to track iodine oxidation and reduction, including to intermediate species, and thus elucidate mechanisms and rates. Rates and mechanisms of I^- oxidation at conditions approximating actual seawater are particularly elusive due to perceived slow reactions and few published experimental constraints. To date, I^- oxidation rates under normal marine conditions have been limited to mass balance approaches (Table 1). For our experiments, we specifically combined the IO_3^- and DOI fractions in order to determine rates of I^- oxidation. Because HOI is a precursor to DOI formation (Luther et al., 1995), DOI acts a proxy for HOI in relatively high DOC systems, such as Martha's Vineyard Sound, where DOC concentration up to 114 μM have been observed (Hopkinson et al., 2002).

Each of our seawater experiments yielded increases in R_{OX} as well as decreases in I^- concentrations, which together suggest the likelihood of I^- oxidation to IO_3^- and/or HOI to form DOI (Fig. 7). We use isotope mass balance to determine the contributions of I^- oxidation to the I_{OX} pool. Equation 2 below utilizes the measured constraints of the initial I_{OX} concentration ($^{127}[OX]_i$) measured via ICP-MS and MC-ICP-MS isotope dilution, the measured isotope ratio of I^- at each time point (R_{iodide_t}), and the measured isotope ratio of I_{OX} at each time point (R_{ox_t}). The $^{129}[OX]_i$ is calculated using the measured ($^{127}[OX]_i$) and R_{OX} at t_0.

$$R_{ox_t} = \frac{^{129}[OX]_i + {}^{129}\Delta[iodide]_{t-1} + {}^{129}\Delta[iodide]_t}{^{127}[OX]_i + {}^{127}\Delta[iodide]_{t-1} + {}^{127}\Delta[iodide]_t} \qquad \textit{(Equation 2)}$$

592 $$R_{iodide_t} = \frac{^{129}\Delta[iodide]_t}{^{127}\Delta[iodide]_t} \qquad \textit{(Equation 3)}$$

593

594 The $^{12x}\Delta[iodide]_t$ represent the contributions from oxidiation of I^- for a given isotope from
595 the previous to the current time point. Note that $^{129}\Delta[iodide]_{t-1}$ and $^{127}\Delta[iodide]_{t-1}$ will be
596 zero from t_0 to t_1 and that values calculated for $^{129}\Delta[iodide]_t$ and $^{127}\Delta[iodide]_t$ for the t_1 point
597 will represent *t-1* for the next time point calculation (t_2). Importantly, R_{iodide}, like R_{OX}, can also
598 have multiple inputs (for example IO_3^- reduction to I^-) and temporal changes and hence have the
599 form of Equation 2. However, in the context of the contribution of bulk I^- to R_{OX} during
600 oxidation, the variables $^{129}\Delta[iodide]_t$ and $^{127}\Delta[iodide]_t$ only need to represent the sum of each
601 $^{129}I^-$ and $^{127}I^-$ at a given time point, respectively. This is because the sum of I^-, which includes both
602 $^{127}I^-$ and $^{129}I^-$ accumulated from any source, contributes to R_{OX} during I^- oxidation.

603 By using the Equation 3 to solve for $^{127}\Delta[iodide]_t$ and substitute into Equation 2, one can
604 solve for the only unknown, $^{129}\Delta[iodide]_t$, and subsequently use this value to solve for
605 $^{127}\Delta[iodide]_t$ using Equation 3. This approach assumes that the only input to the I_{OX} pool is I^-
606 oxidation and that $^{127}[OX]_i$ and $^{129}[OX]_i$ stay constant. The sum of $^{129}\Delta[iodide]_t$ and
607 $^{127}\Delta[iodide]_t$ represent the total iodine transferred to the I_{OX} pool from I^- oxidation since the
608 previous time step. The relative change in the concentrations of both isotopes over time
609 determines the rate of I^- oxidation, and thus accounts for any initial offset in ^{129}I in the I_{OX} pool of
610 the spike and ^{127}I contamination. Calculated concentration increases are shown in Fig. 9.

611 Concentrations up to 35 nM of total I_{OX} from I^- oxidation are calculated for the unamended
612 seawater experiments and ~8 nM for the 0.22 μm-filtered, UV-irradiated seawater experiments
613 over the 67-day incubation period. Our incubation experiments do not discern whether the
614 oxidation of I^- occurs completely to IO_3^- or rather to intermediates HOI/I_2, which then can react
615 with DOC to form DOI. However, given the elusiveness of IO_3^- production and that DOC and
616 DOI concentrations are known to be high in coastal waters such as that studied here (Cook et al.,
617 2000; Wong and Cheng, 1998; Wong and Cheng, 2001a; Wong and Cheng, 2001b; Wong and
618 Cheng, 2008), it is most probable that our experiments constrain an integrative net—rather than
619 gross—rate of I^- oxidation to HOI and subsequent reaction to form DOI. For example, net DOI
620 formation, not IO_3^-, has been observed in seasonal studies of the Chesapeake Bay (Wong and
621 Zhang, 2003). Importantly, if true, the rates found here do not completely constrain rates of HOI
622 and I_2 formation, which, in addition to forming DOI or IO_3^-, could volatilize or reduce to reform I^-
623 (Carpenter et al., 2013; Truesdale and Luther, 1995).

624 The determination of I^- oxidation rates is possible from our experiments. However, as the I^-
625 pool was not exhausted in these 67-day experiments, it remains unclear whether the rates proceed
626 as first order or other reaction pathways. We also do not constrain the degree that the reaction rate
627 is dependent on I^- concentrations, DOC (if applicable), or necessary oxidants. Here, we assume a
628 pseudo-zeroth order reaction based on the prolonged accumulation of I^- in our experiments and
629 the ocean generally, thus pointing to the oxidant, catalyst, or DOC as the limiting reagent for
630 oxidation and signal preservation—opposed to I^- itself—over the timescales of our incubations.

631 Our calculations suggest I^- oxidation rates between 118–189 nM/yr for the unamended
632 seawater experiments (Table 1). These I^- oxidation rates fall within a range similar to some found
633 previously using open ocean mass balance approaches for I^- oxidation, which are compared in
634 Table 1. However, we note that given the extremely slow rates of I^- oxidation in seawater
635 estimated from previous studies, rates of advection and mixing between water masses, biological
636 activity, and inputs/outputs are important for understanding the distribution of marine iodine
637 speciation in such calculations (Campos et al., 1997). Our isotope-labeled incubation experiments

avoid these limitations and more directly quantify the specific oxidation of I^-. Regardless, these rates are extremely slow—orders of magnitude slower than IO_3^- reduction rates in low oxygen settings (Amachi et al., 2007; Farrenkopf et al., 1997).

4.3 Preliminary Constraints on Reaction Mechanisms

We also performed treatments that provide some preliminary insight into—but by no means definitely constrain—the mechanisms of I^- oxidation in seawater. Importantly, the observation of variations in I^- oxidation between our treatments demonstrates the potential for additional experimentation regarding the mechanisms of iodine redox transformations in seawater. Our treatments include variations in filtrate sizes and illumination. Though the experiments were designed to track oxidation, we also compare and contrast concentration and isotope data for I^- to consider co-occuring reactions beyond oxidation.

The rates themselves do vary between treatments, which provide insights into potential mechanisms for I^- oxidation. Specifically, Treatments A, B, and C have similar isotopic trends over the first 7 days of the experiment, but only incbuations A and B exhibit continued increases in $^{129}I/^{127}I$ indicative of oxidation through the 67 day incubation time period. We note that, though of a similar magnitude, Treatment A and C had variable specific increases in $^{129}I_{OX}$ between t_0 and t_1 (3.3 ± 1.7 and 7.6 ± 1.6 nM, respectively). The sustained oxidation observed in Treatments A and B (raw and sand-filtered seawater) relative to the "kill treatment", incubation C (0.22 μm, UV-irradiated seawater), provides preliminary evidence that both abiotic and biotic process are responsible for I^- oxidation, but that sustained I_{OX} production (from I^- oxidation) likely requires a biotic mechanism. This is true in both light and dark experiments, which varied for some indivual time points, but not as a whole. The light-incubated samples of Incubation A do consistently show higher $^{129}I/^{127}I$ relative to dark-incubated samples for all replicates of the unamended seawater experiments, but similar observations are not observed for the other treatments, which would be expected for this abiotic reaction. In general, the observation of only ~8 nM I^- oxidation in the filtered treatment C is within the measurement error of previous studies reporting prolonged iodine speciation stability in filtered, sealed vials for timescales up to years (Hou et al., 2001; Smith et al., 1990; Campos, 1997; Farrenkopf et al., 1997; Jickells et al., 1988).

Though we cannot confirm the actual oxidant(s), one mechanism for the I^- oxidation in all seawater treatments, including Incubation C, might be enzymes which could directly oxidize I^- or produce reactive oxygen species (ROS) in the medium. For oxidation, the ROS superoxide and hydrogen peroxide have been demonstrated or shown favorable to oxidize I^- in artificial seawater mediums and could play a role in our observations (Luther et al., 1995; Li et al., 2014). Hydrogen peroxide and superoxide production have even been demonstrated in 0.2 μm filtered, irradiated seawater from Martha's Vineyard Sound (Moffett and Zafiriou, 1990), our same sampling location. Regardless, this possibility suggests that filtered, aged seawater—where enzymatic ROS production had ceased (Roe et al., 2016)—would be more appropriate for "kill treatments" in future experiments. Other biotic mechanisms are possible, for example I^- oxidation has been demonstrated to be catalyzed by bacteria in brines (Amachi et al., 2005).

Another clue to oxidation mechanisms comes from differences of I^- lost from the incubations measured via I^- concentrations relative to I^- oxidation rates derived from the R_{OX} values (Figures 7, 8, 9). The loss of I^- cannot be explained by oxidation of I^- to I_{OX}, because this would require the I_{OX} concentration to have increased by up to 300 nM, which is far below what was observed in the experiments (Fig. 9). Although the I^- concentrations measured by ICP-MS are significantly less precise than what would be desired for quantifying I^- loss from the experiments, the fact that we consistently observed loss of I^- in the majority of the experiments where $[I^-]$ was monitored likely points to loss processes occurring during the experiments themselves. We consider loss via (ad)sorption to exogenous particulates or other macro-materials as unlikely given the lack of clear difference in trends between unfiltered (Treatment A) and those that were filtered to 0.22 μm (Treatment C). Though this does not rule out I^- loss to particles endogenously formed over the

course of the experiments, we consider the most likely loss process to be oxidation to gaseous I_2 and HOI that is then lost to the atmosphere (Bichsel and Von Gunten, 1999; Carpenter et al., 2013; Garland and Curtis, 1981; Küpper et al., 2008; Martino et al., 2009; Shaw and Carpenter, 2013; MacDonald et al., 2014; Sherrill et al., 2004). Given up to 300 nM I^- loss from our 10 mL experiments (2.5 cm diameter vial), this is generally equivalent to ~90 nmol m^{-2} day^{-1} flux of I^- from the solution. This is in the range of <800 nmol m^{-2} day^{-1} flux modeled for Atlantic and Pacific surface waters in previous studies (Carpenter et al., 2013; MacDonald et al., 2014). Importantly, we recognize that our experiments did not ideally replicate ocean surface conditions, and hence the model comparison is strictly qualitative. Nonetheless, these calculations demonstrate the feasibility of this loss mechanism in contributing to I^- loss over the course of the experiments.

Lastly, the isotopic composition of I^- strongly implies that an external source of $^{127}I^-$ was added during the incubations, even as I^- concentrations decline (Figure 8a,b). This change in $^{129}I/^{127}I$ could be explained either by isotopic exchange between DOI/IO_3^- and I^-, the *in situ* reduction of IO_3^- in the experiments, or imply addition of an external source of ^{127}I to the experiments. Based on multiple lines of evidence we conclude that neither isotopic exchange between DOI/IO_3^- and I^- or that IO_3^- reduction are likely to have taken place. For example, some experiment time points were filtered, capped, and refrigerated for long time periods before chromatographic separation of the iodine species. These reveal no difference to identical experiment time points that had not been stored (Fig. 8b). Also, the decrease in R_{iodide} was observed even in Incubation D—^{129}I spiked 18.2 MΩ cm^{-2}-grade H_2O— which lacks sufficient IO_3^- to explain the R_{iodide} via isotopic exchange or IO_3^- reduction. Further, in the experiments, IO_3^-/DOI concentrations show no substantial changes indicative of IO_3^- reduction (Supplementary Table 1). Therefore, the decrease in R_{iodide} must be due to external addition of $^{127}I^-$ to the experiments. The added I^- may represent contamination from the vials or the laboratory, and, given that the vial headspace was permitted to exchange with the external atmosphere, it could also be associated with atmospheric iodine gases. We cannot explicitly rule out or confirm an influence of atmospheric iodine sources, but we note that these include oxidized and reduced as well as organic and inorganic forms of iodine (e.g., Gilfedder et al., 2008), while this phenomenon was only clearly observed with I^- in our samples. We can constrain however the required external $^{127}I^-$ addition to explain the R_{iodide} values. Calculations utilizing the measured R_{iodide} at t_0 and the time point of interest and the measured $^{127}I^-$ reveal that an external source, if present, would require the total addition of 66±31 and 37±26 nM $^{127}I^-$ to explain the final data points from Treatments A and C, respectively. Regardless, we note that ^{129}I is at too low of natural abundances to represent a contamination threat and that the increases in the R_{OX} over the experiments provide strong evidence for I^- oxidation to I_{OX}.

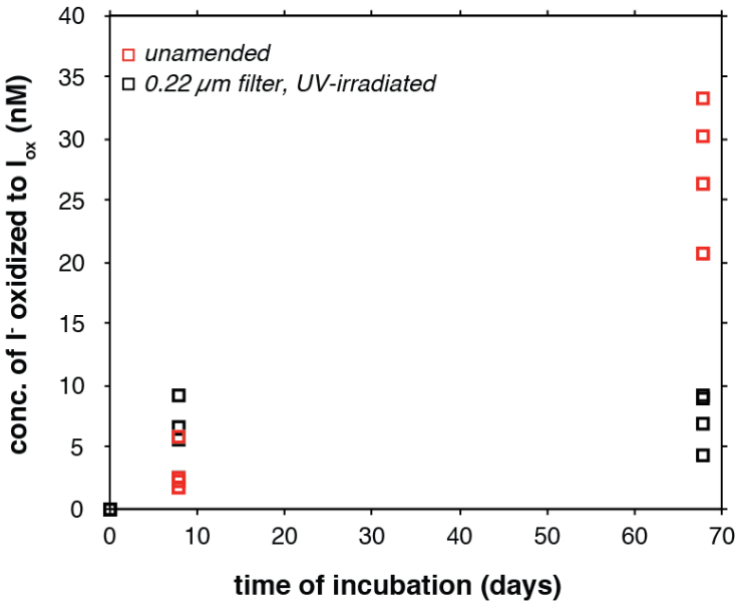

Fig. 9. Calculated concentrations of I_{OX} derived from I^- oxidation in seawater both unamended and 0.22 µm-filtered, UV-irradiated. Incubations done in the light versus dark are not distinguished. Error bars represent 3σ of t_0 samples for each incubation and are smaller than data points.

4.4 Implications for iodine speciation as a tracer

Our experimental observation of slow I^- oxidation rates in seawater are consistent with well-known observations of prolonged I^- accumulation in well-oxygenated seawater and thermodynamic considerations that provide evidence that I^- oxidation is catalyzed by microbial organisms and/or requires relatively low abundance reactive oxygen species such as ozone, hydrogen peroxide, or superoxide (Carpenter et al., 2013; Li et al., 2014; Li et al., 2012; Luther et al., 1995; Sherrill et al., 2004). Given the extreme slow I^- oxidation rates in seawater, some studies have postulated that I^- itself may act as a tracer of water mass sources (Cutter et al., 2018; Farrenkopf and Luther, 2002). For example, observations of elevated I^- relative to typical total inorganic iodine concentrations along continental margins have been linked to a pore fluid I^- source. At the Eastern Tropical South Pacific oxygen minimum zone, µM levels of I^- have been linked to elevated ^{228}Ra, a sedimentary pore fluid tracer (Cutter et al., 2018). It is well known that pore waters can have up to several µM or more levels of I^- derived from the oxidation of organic carbon during diagenesis (Anschutz et al., 2000; Kennedy and Elderfield, 1987a; Kennedy and Elderfield, 1987b; Ullman and Aller, 1985), which have typical I/C ratios near 10^{-4} (Elderfield and Truesdale, 1980). These pore fluid concentrations are several orders of magnitude greater than the 450 nM of total dissolved iodine found in typical seawater. Our data here support the application of I^- as a tracer, but, importantly, provide quantitative constraints on its application through the empirical determination of I^- oxidation rates. These rates are necessary for detailed consideration of the ages of water masses for which externally sourced I^- may be considered as a tracer.

Our data provide direct constraints to iodine cycle models used in association with iodine-to-calcium ratios. I/Ca ratios in ancient carbonates have been applied as a tracer of past marine IO_3^- accumulation (Hardisty et al., 2017; Hardisty et al., 2014; Hoogakker et al., 2018; Lowery et al., 2018; Lu et al., 2018; Lu et al., 2016; Lu et al., 2010). Indeed, the use of carbonate I/Ca ratios in 2.4 Ga carbonates across the Great Oxidation Event reveals the onset of IO_3^-

accumulation in association with independent evidence for a major redox transition (Hardisty et al., 2014). In combination with detailed models of the global marine iodine cycle, the distribution of past marine IO_3^- is interpreted to reflect the degree of OMZ-analogue conditions in regional ocean basins where IO_3^- is reduced to I^- in the water column during organic matter remineralization (Farrenkopf et al., 1997). The slow I^- oxidation kinetics will allow for the dispersion of IO_3^- deficient waters even beyond the sites of *in situ* IO_3^- reduction. To date, these studies have relied on estimates of I^- oxidation rates based on the seasonal mass balance and less direct approaches like those outlined in Table 1. Though we ultimately conclude that our rate estimations are similar in magnitude to these past studies, considerations of the more direct rate estimations outlined here will be crucial to refine such models. For example, global iodine cycling models demonstrating the potential of OMZ oxycline depth as a control on shallow ocean IO_3^- during Paleozoic and older time periods conservatively relied on the slowest I^- oxidation rates in Table 1 (Lu et al., 2018), while our data suggest that two orders of magnitude faster rates may be applicable. Important to these considerations will be future experiments with controls and treatments specifically discriminating between I^- oxidation and IO_3^- production rates. Regardless, our study generally supports I/Ca interpretations linking low ratios from carbonate deposited within near surface waters—and hence low surface ocean dissolved IO_3^-—to the presence of a shallow chemocline or mixing with adjacent water masses either actively supporting or preserving signals of IO_3^- reduction. This is opposed to interpretations relating I/Ca to specific O_2 concentrations, as *in situ* oxidation is likely too slow to support any reproducible IO_3^-–O_2 relationship.

Location	Rate	Method	Source
Martha's Vineyard Sound	118-189 nM/yr	^{129}I doped seawater incubations	This study
NE Atlantic surface waters	1.5-8.2 nM/yr	open ocean $^{129}I/^{127}I$ of I^- and IO_3^-	(He et al., 2013)
Pacific	0.025 yr^{-1}	mass balance of N. Pacific seawater transects	(Tsunogai, 1971)
Black Sea surface waters	8 nM/yr	basinal iodine mass balance	(Truesdale et al., 2001)
Loch Etive, Scotland	30 nM/yr	seasonal iodine speciation changes	(Edwards and Truesdale, 1997)
Croatian marine cave	550 nM/yr	seasonal iodine speciation changes	(Žic and Branica, 2006; Žic et al., 2008)
Pacific gyre	560 nM/yr	seasonal iodine speciation changes	(Campos et al., 1996)
Atlantic gyre	270 nM/yr	seasonal iodine speciation changes	(Campos et al., 1996)

Table 1. Estimated oxidation rates of I^- from this work previous approaches**.**

5. Conclusions

We provide evidence for marine oxidation of the reduced iodine species, I^-. Direct observations of this process have been elusive in past seawater studies, largely due to a focus on open ocean mass balance and a dearth of experimental work replicating normal marine conditions. Our observations come from incubation experiments where ^{129}I, which has an extreme low natural abundance in nature, was added to seawater (10 mL) as I^- at concentrations comparable to observations under normal marine conditions. Such a method allows that increases in the isotope ratio of ^{129}I relative to ^{127}I—the only stable iodine isotope—in IO_3^- and DOI can be exclusively linked to I^- oxidation. In an effort to detect ^{129}I even at low abundances, we developed a novel sparge-introduction system of iodine gas into a MC-ICP-MS. The sparge method increases transmission efficiency of iodine by ~10× relative to wet plasma and we demonstrate that relative signal intensities of iodine isotopes can be increased even further through increases in sparged-sample volume. The sparge approach outlined here provides utility in experimental constraints on iodine reduction and oxidation, even at slow rates, but also as an isotope dilution technique for characterizing ^{127}I concentration in a range of materials. Iodide oxidation was

observed even in 0.22 μm-filtered samples, but prolonged oxidation was exclusive to unfiltered or low-mesh filtered samples. Rates of I^- oxidation in unfiltered seawater ranged from 118–189 nM/yr which is comparable to some previous open-ocean mass balance calculations. Ultimately, the extreme slow oxidation kinetics of I^- suggest that *in situ* processes are unlikely to dominate local iodine speciation, but instead that iodine speciation is a powerful regional-scale water mass tracer in both modern and ancient seawater.

6. Acknowledgments

This research was made possible by a WHOI Postdoctoral Scholarship (awarded to D.S.H.), WHOI Institutional support (provided to T.J.H. and S.G.N.), and the NSF Chemical Oceanography Award #1829406 granted to D.S.H. and S.G.N. Thanks go to M. Auro for keeping the lab running smoothly. We acknowledge the use of the NSF-supported WHOI Plasma Facility and thank G. Swarr for assistance. This manuscript benefited immensely from the thoughtful comments of three anonymous reviewers.

7. References

Amachi, S., Muramatsu, Y., Akiyama, Y., Miyazaki, K., Yoshiki, S., Hanada, S., Kamagata, Y., Ban-nai, T., Shinoyama, H. and Fujii, T., 2005. Isolation of iodide-oxidizing bacteria from iodide-rich natural gas brines and seawaters. Microbial ecology: 49(4), 547-557.

Amachi, S. et al., 2007. Dissimilatory iodate reduction by marine Pseudomonas sp. strain SCT. Applied and environmental microbiology, 73(18): 5725-5730.

Anschutz, P., Sundby, B., Lefrancois, L., Luther, G.W., Mucci, A., 2000. Interactions between metal oxides and species of nitrogen and iodine in bioturbated marine sediments. Geochimica et Cosmochimica Acta, 64(16): 2751-2763.

Audi, G., Bersillon, O., Blachot, J., Wapstra, A., 2003. The NUBASE evaluation of nuclear and decay properties. Nuclear Physics A, 729(1): 3-128.

Belshaw, N., Freedman, P., O'nions, R., Frank, M., Guo, Y., 1998. A new variable dispersion double-focusing plasma mass spectrometer with performance illustrated for Pb isotopes. International Journal of Mass Spectrometry, 181(1-3): 51-58.

Berry, F.J., Collins, R.D., Parish, R., Moore, L.S., 1987. Studies of iodine in nitric acid and of iodine adsorbed onto silver-impregnated silica. Inorganica chimica acta, 126(1): 119-124.

Bichsel, Y., Von Gunten, U., 1999. Oxidation of iodide and hypoiodous acid in the disinfection of natural waters. Environmental science & technology, 33(22): 4040-4045.

Brandão, A.C.M., Wagener, A.d.L.R., Wagener, K., 1994. Model experiments on the diurnal cycling of iodine in seawater. Marine Chemistry, 46(1-2): 25-31.

Buesseler, K. et al., 2017. Fukushima Daiichi–derived radionuclides in the ocean: transport, fate, and impacts. Annual review of marine science, 9: 173-203.

Campos, M., Farrenkopf, A., Jickells, T., Luther, G., 1996. A comparison of dissolved iodine cycling at the Bermuda Atlantic Time-series Station and Hawaii Ocean Time-series Station. Deep Sea Research Part II: Topical Studies in Oceanography, 43(2): 455-466.

Campos, M.L.A., 1997. New approach to evaluating dissolved iodine speciation in natural waters using cathodic stripping voltammetry and a storage study for preserving iodine species. Marine Chemistry, 57(1-2): 107-117.

Carpenter, L.J. et al., 2013. Atmospheric iodine levels influenced by sea surface emissions of inorganic iodine. Nature Geoscience, 6(2): 108-111.

Chai, J.Y., Muramatsu, Y., 2007. Determination of bromine and iodine in twenty-three geochemical reference materials by ICP-MS. Geostandards and Geoanalytical Research, 31(2): 143-150.

Chance, R., Baker, A.R., Carpenter, L., Jickells, T.D., 2014. The distribution of iodide at the sea surface. Environmental Science: Processes & Impacts, 16: 1841-1859.

Cook, P.L., Carpenter, P.D., Butler, E.C., 2000. Speciation of dissolved iodine in the waters of a humic-rich estuary. Marine Chemistry, 69(3-4): 179-192.

Cutter, G.A., Moffett, J.G., Nielsdóttir, M.C., Sanial, V., 2018. Multiple oxidation state trace elements in suboxic waters off Peru: In situ redox processes and advective/diffusive horizontal transport. Marine Chemistry, 201: 77-89.

de Laeter, J.R. et al., 2003. Atomic weights of the elements. Review 2000 (IUPAC Technical Report). Pure and applied chemistry, 75(6): 683-800.

Dugdale, R., Goering, J., 1967. Uptake of new and regenerated forms of nitrogen in primary productivity. Limnology and oceanography, 12(2): 196-206.

Edwards, A., Truesdale, V., 1997. Regeneration of inorganic iodine species in Loch Etive, a natural leaky incubator. Estuarine, Coastal and Shelf Science, 45(3): 357-366.

Elderfield, H., Truesdale, V.W., 1980. On the biophilic nature of iodine in seawater. Earth and Planetary Science Letters, 50(1): 105-114.

Farrenkopf, A.M., Dollhopf, M.E., Chadhain, S.N., Luther, G.W., Nealson, K.H., 1997. Reduction of iodate in seawater during Arabian Sea shipboard incubations and in laboratory cultures of the marine bacterium *Shewanella putrefaciens* strain MR-4. Marine Chemistry, 57(3): 347-354.

Farrenkopf, A.M., Luther, G.W., 2002. Iodine chemistry reflects productivity and denitrification in the Arabian Sea: evidence for flux of dissolved species from sediments of western India into the OMZ. Deep Sea Research Part II: Topical Studies in Oceanography, 49(12): 2303-2318.

Feng, X., Redfern, S.A., 2018. Iodate in calcite, aragonite and vaterite CaCO3: Insights from first-principles calculations and implications for the I/Ca geochemical proxy. Geochimica et Cosmochimica Acta, 236: 351-360.

Fox, P.M., Davis, J.A., Luther, G.W., 2009. The kinetics of iodide oxidation by the manganese oxide mineral birnessite. Geochimica et Cosmochimica Acta, 73(10): 2850-2861.

Garland, J., Curtis, H., 1981. Emission of iodine from the sea surface in the presence of ozone. Journal of Geophysical Research: Oceans, 86(C4): 3183-3186.

Gilfedder, B.S., S.C. Lai, M. Petri, H. Biester, Hoffmann, T., 2008, Iodine speciation in rain, now and aerosols. *Atmospheric Chemistry and Physic,s* 8: 6069-6084.

Hansen, V. et al., 2011. Iodide and iodate (129 I and 127 I) in surface water of the Baltic Sea, Kattegat and Skagerrak. Science of the Total Environment, 412: 296-303.

Hardisty, D.S. et al., 2017. Perspectives on Proterozoic surface ocean redox from iodine contents in ancient and recent carbonate. Earth and Planetary Science Letters, 463: 159-170.

875 Hardisty, D.S. et al., 2014. An iodine record of Paleoproterozoic surface ocean oxygenation.
876 Geology, 42: 619-622.

877 He, P., Hou, X., Aldahan, A., Possnert, G., Yi, P., 2013. Iodine isotopes species fingerprinting
878 environmental conditions in surface water along the northeastern Atlantic Ocean.
879 Scientific reports, 3: 2685.

880 Hoogakker, B.A.A. et al., 2018. Glacial expansion of oxygen-depleted seawater in the eastern
881 tropical Pacific. Nature, 562(7727): 410-413.

882 Hopkinson Jr, C.S., Vallino, J.J. and Nolin, A., 2002, Decomposition of dissolved organic matter
883 from the continental margin. Deep Sea Research Part II: Topical Studies in
884 Oceanography, 49(20): 4461-4478.

885 Horner, T.J., Kinsley, C.W., Nielsen, S.G., 2015. Barium-isotopic fractionation in seawater
886 mediated by barite cycling and oceanic circulation. Earth and Planetary Science Letters,
887 430: 511-522.

888 Hou, X. et al., 2007. Speciation of 129I and 127I in seawater and implications for sources and
889 transport pathways in the North Sea. Environmental Science & Technology, 41(17):
890 5993-5999.

891 Hou, X., Aldahan, A., Nielsen, S.P., Possnert, G.r., 2009. Time series of 129I and 127I speciation
892 in precipitation from Denmark. Environmental Science & Technology, 43(17): 6522-
893 6528.

894 Hou, X., Dahlgaard, H., Nielsen, S., 2001. Chemical speciation analysis of 129 I in seawater and
895 a preliminary investigation to use it as a tracer for geochemical cycle study of stable
896 iodine. Marine Chemistry, 74(2): 145-155.

897 Hou, X. et al., 1999. Determination of chemical species of iodine in seawater by radiochemical
898 neutron activation analysis combined with ion-exchange preseparation. Analytical
899 Chemistry, 71(14): 2745-2750.

900 Hou, X. et al., 2013. Iodine-129 in seawater offshore Fukushima: distribution, inorganic
901 speciation, sources, and budget. Environmental Science & Technology, 47(7): 3091-
902 3098.

903 Isnard, H., Nonell, A., Marie, M., Chartier, F., 2016. Accurate measurements of 129I
904 concentration by isotope dilution using MC-ICPMS for half-life determination.
905 Radiochimica Acta, 104(2): 131-139.

906 Jickells, T.D., Boyd, S.S., & Knap, A.H., 1988, Iodine cycling in the Sargasso Sea and the
907 Bermuda inshore waters. *Marine Chemistry*: *24*, 61-82.

908 Jørgensen, B.B., 1982. Mineralization of organic matter in the sea bed—the role of sulphate
909 reduction. Nature, 296: 643-645.

910 Kennedy, H., Elderfield, H., 1987a. Iodine diagenesis in non-pelagic deep-sea sediments.
911 Geochimica et Cosmochimica Acta, 51(9): 2505-2514.

912 Kennedy, H., Elderfield, H., 1987b. Iodine diagenesis in pelagic deep-sea sediments. Geochimica
913 et Cosmochimica Acta, 51(9): 2489-2504.

914 Kerisit, S. et al., 2018. Incorporation Modes of Iodate in Calcite. Environmental Science &
915 Technology, *52*: 5902-5910.

916 Kerl, W., áSabine Becker, J., Dietz, H., Dannecker, W., 1996. Determination of iodine using a
917 special sample introduction system coupled to a double-focusing sector field inductively

coupled plasma mass spectrometer. Journal of Analytical Atomic Spectrometry, 11(9): 723-726.

Küpper, F.C. et al., 2008. Iodide accumulation provides kelp with an inorganic antioxidant impacting atmospheric chemistry. Proceedings of the National Academy of Sciences, 105(19): 6954-6958.

Li, H.-P. et al., 2014. Superoxide production by a manganese-oxidizing bacterium facilitates iodide oxidation. Applied and Environmental Microbiology, 80(9): 2693-2699.

Li, H.-P. et al., 2012. Bacterial production of organic acids enhances H2O2-dependent iodide oxidation. Environmental Science & Technology, 46(9): 4837-4844.

Lowery, C.M. et al., 2018. Rapid recovery of life at ground zero of the end-Cretaceous mass extinction. Nature, 558: 288–291

Lu, W.Y. et al., 2018. Late inception of a resiliently oxygenated upper ocean. Science, 361(6398): 174-177.

Lu, Z. et al., 2016. Oxygen depletion recorded in upper waters of the glacial Southern Ocean. Nature Communications, 7.

Lu, Z., Jenkyns, H.C., Rickaby, R.E., 2010. Iodine to calcium ratios in marine carbonate as a paleo-redox proxy during oceanic anoxic events. Geology, 38(12): 1107-1110.

Luther, G.W., Campbell, T., 1991. Iodine speciation in the water column of the Black Sea. Deep Sea Research Part A. Oceanographic Research Papers, 38: S875-S882.

Luther, G.W., Wu, J., Cullen, J.B., 1995. Redox Chemistry of Iodine in Seawater: Frontier Molecular Orbital Theory Considerations. Aquatic chemistry: interfacial and interspecies processes, 244: 135.

MacDonald, S.M., Gómez Martín, J.C., Chance, R., Warriner, S., Saiz-Lopez, A., Carpenter, L. J., & Plane, J.M.C., 2014, A laboratory characterisation of inorganic iodine emissions from the sea surface: dependence on oceanic variables and parameterisation for global modelling. Atmospheric Chemistry and Physics: 14: 5841-5852.

Martino, M., Mills, G.P., Woeltjen, J., Liss, P.S., 2009. A new source of volatile organoiodine compounds in surface seawater. Geophysical Research Letters, 36(1).

Moffett, J.W., 1990. Microbially mediated cerium oxidation in sea water. Nature, 345: 421-423.

Moffett, J.W., Ho, J., 1996. Oxidation of cobalt and manganese in seawater via a common microbially catalyzed pathway. Geochimica et Cosmochimica Acta, 60(18): 3415-3424.

Moffett, J.W., & Zajiriou, O.C., 1990, An investigation of hydrogen peroxide chemistry in surface waters of Vineyard Sound with $H_2{}^{18}O_2$ and $^{18}O_2$. Limnology and Oceanography: 35(6), 1221-1229.

Ohno, T. et al., 2013. Determination of ultratrace 129 I in soil samples by Triple Quadrupole ICP-MS and its application to Fukushima soil samples. Journal of Analytical Atomic Spectrometry, 28(8): 1283-1287.

Podder, J. et al., 2017. Iodate in calcite and vaterite: Insights from synchrotron X-ray absorption spectroscopy and first-principles calculations. Geochimica et Cosmochimica Acta, 198: 218-228.

Reifenhäuser, C., Heumann, K.G., 1990. Development of a definitive method for iodine speciation in aquatic systems. Fresenius' Journal of Analytical Chemistry, 336(7): 559-563.

961 Remenec, B., Dulanská, S., Horváthová, B., Mátel, Ľ., 2017. Determination of 129I using
962 volatilization method and liquid scintillation spectrometry. Journal of Radioanalytical and
963 Nuclear Chemistry: 311(3): 1649-1655.

964 Roe, K.L., Schneider, R.J., Hansel, C.M., & Voelker, B.M., 2016, Measurement of dark,
965 particle-generated superoxide and hydrogen peroxide production and decay in the
966 subtropical and temperate North Pacific Ocean. Deep Sea Research Part I. Oceanographic
967 Research Papers: 107: 59-69.

968 Rue, E.L., Smith, G.J., Cutter, G.A., Bruland, K.W., 1997. The response of trace element redox
969 couples to suboxic conditions in the water column. Deep Sea Research Part I:
970 Oceanographic Research Papers, 44(1): 113-134.

971 Santamaria-Fernandez, R., Evans, P., Wolff-Briche, C.S., Hearn, R., 2006. A high accuracy
972 primary ratio method for the determination of iodine in complex matrices by double
973 isotope dilution using MC-ICPMS and 129 I spike. Journal of Analytical Atomic
974 Spectrometry, 21(4): 413-421.

975 Santschi, P. et al., 2017. Recent advances in the detection of specific natural organic compounds
976 as carriers for radionuclides in soil and water environments, with examples of radioiodine
977 and plutonium. Journal of Environmental Radioactivity, 171: 226-233.

978 Schwehr, K.A., Santschi, P.H., Elmore, D., 2005. The dissolved organic iodine species of the
979 isotopic ratio of 129I/127I: a novel tool for tracing terrestrial organic carbon in the
980 estuarine surface waters of Galveston Bay, Texas. Limnology and Oceanography:
981 Methods, 3(8): 326-337.

982 Sen, I.S., Peucker-Ehrenbrink, B., 2014. Determination of osmium concentrations and
983 187Os/188Os of crude oils and source rocks by coupling high-pressure, high-temperature
984 digestion with sparging OsO4 into a multicollector inductively coupled plasma mass
985 spectrometer. Analytical Chemistry, 86(6): 2982-2988.

986 Shaw, M.D., Carpenter, L.J., 2013. Modification of Ozone Deposition and I_2 Emissions at the
987 Air–Aqueous Interface by Dissolved Organic Carbon of Marine Origin. Environmental
988 Science & Technology, 47(19): 10947-10954.

989 Sherrill, J., Whitaker, B.R., Wong, G.T., 2004. Effects of ozonation on the speciation of dissolved
990 iodine in artificial seawater. Journal of Zoo and Wildlife Medicine, 35(3): 347-355.

991 Smith, J.D., Butler, E.C., Airey, D., Sandars, G., 1990. Chemical properties of a low-oxygen
992 water column in Port Hacking (Australia): arsenic, iodine and nutrients. Marine
993 Chemistry, 28(4): 353-364.

994 Truesdale, V.W., 1974. The chemical reduction of molecular iodine in seawater, Deep Sea
995 Research and Oceanographic Abstracts. Elsevier, pp. 761-766.

996 Truesdale, V.W., Luther, G.W., 1995. Molecular iodine reduction by natural and model organic
997 substances in seawater. Aquatic Geochemistry, 1(1): 89-104.

998 Truesdale, V.W., Watts, S.F., Rendell, A., 2001. On the possibility of iodide oxidation in the
999 near-surface of the Black Sea and its implications to iodine in the general ocean. Deep
1000 Sea Research Part I: Oceanographic Research Papers, 48(11): 2397-2412.

1001 Tsunogai, S., 1971. Iodine in the deep water of the ocean, Deep Sea Research and Oceanographic
1002 Abstracts. Elsevier, pp. 913-919.

1003 Ullman, W.J., Aller, R.C., 1985. The geochemistry of iodine in near-shore carbonate sediments.
1004 Geochimica et Cosmochimica Acta, 49(4): 967-978.

1005 Wong, G.T., Brewer, P.G., 1976. The determination of iodide in sea water by neutron activation
1006 analysis. Analytica Chimica Acta, 81(1): 81-90.

1007 Wong, G.T., Brewer, P.G., 1977. The marine chemistry of iodine in anoxic basins. Geochimica et
1008 Cosmochimica Acta, 41(1): 151-159.

1009 Wong, G.T., Cheng, X.-H., 1998. Dissolved organic iodine in marine waters: determination,
1010 occurrence and analytical implications. Marine Chemistry, 59(3-4): 271-281.

1011 Wong, G.T., Cheng, X.-H., 2001a. Dissolved organic iodine in marine waters: role in the
1012 estuarine geochemistry of iodinePresented at the Whistler 2000 Speciation Symposium,
1013 Whistler Resort, BC, Canada, June 25–July 1, 2000. Journal of Environmental
1014 Monitoring, 3(2): 257-263.

1015 Wong, G.T., Cheng, X.-H., 2001b. The formation of iodide in inshore waters from the
1016 photochemical decomposition of dissolved organic iodine. Marine Chemistry, 74(1): 53-
1017 64.

1018 Wong, G.T., Cheng, X.-H., 2008. Dissolved inorganic and organic iodine in the Chesapeake Bay
1019 and adjacent Atlantic waters: Speciation changes through an estuarine system. Marine
1020 Chemistry, 111(3-4): 221-232.

1021 Wong, G.T., Takayanagi, K., Todd, J.F., 1985. Dissolved iodine in waters overlying and in the
1022 Orca Basin, Gulf of Mexico. Marine Chemistry, 17(2): 177-183.

1023 Wong, G.T. and Zhang, L.S., 2003. Seasonal variations in the speciation of dissolved iodine in
1024 the Chesapeake Bay. Estuarine, Coastal and Shelf Science, *56*: 1093-1106.

1025 Wong, G.T., Zhang, L.-S., 2008. The kinetics of the reactions between iodide and hydrogen
1026 peroxide in seawater. Marine Chemistry, 111(1-2): 22-29.

1027 Xu, C. et al., 2013. Novel molecular-level evidence of iodine binding to natural organic matter
1028 from Fourier transform ion cyclotron resonance mass spectrometry. Science of the Total
1029 Environment, 449: 244-252.

1030 Yeager, C.M. et al., 2017. Microbial Transformation of Iodine: From Radioisotopes to Iodine
1031 Deficiency, Advances in Applied Microbiology. Elsevier, pp. 83-136.

1032 Zhou, X. et al., 2017. Organically bound iodine as a bottom-water redox proxy: Preliminary
1033 validation and application. Chemical Geology: 95-106.

1034 Žic, V., Branica, M., 2006. The distributions of iodate and iodide in Rogoznica Lake (East
1035 Adriatic Coast). Estuarine, Coastal and Shelf Science, 66(1): 55-66.

1036 Žic, V., Truesdale, V.W., Cukrov, N., 2008. The distribution of iodide and iodate in anchialine
1037 cave waters—Evidence for sustained localised oxidation of iodide to iodate in marine
1038 water. Marine Chemistry, 112(3-4): 168-178.